Coupled coherent and incoherent motion of triplet excitons: Influence on the ESR line shape of pairs of differently oriented molecules

P. Reineker
Abteilung für Theoretische Physik I, University of Ulm, Oberer Eselsberg, 7900 Ulm, Germany
(Received 30 November 1977)

The ESR line shape of triplet excitons, moving in a coupled coherent and incoherent manner within a pair of differently oriented molecules, is calculated. The dynamics of the electronic degrees of freedom is described by the Hamiltonian of the Haken-Strobl model, which consists of a time-independent part, determining the coherent exciton motion via the exchange-interaction integral J between the molecules, and of a stochastically-time-dependent part. The latter part takes into account the influence of the phonons by fluctuations of the energy of the localized excitation (strength γ_0) and of the exchange-interaction integral (strength γ_1) and represents the incoherent part of the motion. The spin Hamiltonian constains the Zeeman energy of the spin in an external magnetic field and the fine-structure terms of the two differently oriented molecules. The eigensolutions of the Liouville equation for the density operator are calculated using parameter values fitting the naphthalene AB pair; their dependence of γ_0 and γ_1 is discussed. From linear-response theory the ESR line shape is determined using the eigensolutions of the Liouville equation. It is shown that from this model the ESR line shape is obtained not only for the cases of the completely coherent and the purely hopping motion of the exciton, as well as for the case of its complete localization on the A and B molecules, but also for all cases in between depending on the relative magnitude of the exchange-interaction integral J and of the strengths γ_0 and γ_1 of the local and nonlocal fluctuations.

I. INTRODUCTION

In recent years, a series of experimental and theoretical papers has been concerned with the question of whether excitons[1] in molecular crystals[2] move coherently or incoherently. Various experimental methods have been applied to a number of systems in investigating this problem.

Meanwhile, there is no question that ESR measurements at triplet excitons in single crystals of naphthalene[3-5] and anthracene[3-5,6] at room temperature have to be interpreted[7] in the incoherent picture. In these materials triplet excitons move predominantly in the a-b plane of the crystal via a hopping process with an effective hopping rate,[8] which is also influenced by the coherent part of the exciton motion.

Whereas in naphthalene and anthracene the exciton motion is two dimensional, in some salts of tetracyanoquinodimethane[9] (TCNQ) the hopping of the excitations occurs in one dimension. Also for 1,4-dibromonaphthalene it has been shown by optical[10-12] and ESR measurements[13] that triplet excitons move mainly along linear chains of molecules oriented in the same way. Furthermore, below 16 K the exciton motion is assumed to be coherent.[13,14] In single crystals of 1,2,4,5-tetrachlorobenzene the exciton motion is also one dimensional, and optically detected magnetic resonance (ODMR) and optical measurements at low temperatures have been discussed in the coherent-exciton model.[15-17] In these papers the theoretical results of Sternlicht and McConnel[18] have been generalized by taking into account the selectivity of the spin-orbit coupling.[19]

Pairs of translationally equivalent molecules of 1,4-dibromonaphthalene-h_6 in the perdeutero host have been investigated optically with ODMR by Hochstrasser and Zewail[20] and pairs of 1,2,4,5-tetrachlorobenzene-h_2 in the perdeutero host by Zewail and Harris[21,22] at a temperature of about 1.5 K. The results of these experiments have also been interpreted within the model of the coherent-exciton motion with the help of the selective spin-orbit interaction, and relations between the parameters of the two-molecule system and those of a linear chain of molecules have been derived. Only recently, in crystals of naphthalene-d_8 doted with naphthalene-h_8 triplet excitons in pairs of translationally equivalent molecules of naphthalene-h_8 (AA pairs) have been observed both optically[23] and by magnetic resonance.[24]

In the same system triplet excitons in pairs of translationally inequivalent naphthalene-h_8 molecules (AB pairs), formed by the two differently oriented molecules in the unit cell of naphthalene crystals, have been detected by Schwoerer and Wolf[25,26] using ESR, soon after the identification of the long-lived excited state of single naphthalene molecules in a durene matrix as a triplet state by Hutchison and Mangum.[27] The ESR results of Schwoerer and Wolf have been discussed[28] using the hopping model of the exciton motion. From optical measurements[29,30] at such doted naphthalene crystals it has been conjectured[31,32] that excitons in the AB pair should possibly be described within the coherent model. The final confirmation

that the coherent description applies has been derived by Botter *et al.*[33] from ODMR and spin-echo measurements using a model of van 't Hof and Schmidt[34] for the interpretation of their results. Recent ESR measurements of Hinkel[35] at the same system have been discussed[36] in the coherent model of the exciton motion taking into account an inhomogeneous distribution of the energy levels of the pair.

For the theoretical description of the exciton motion in molecular crystals, Haken and Strobl[37-39] developed a model, which takes into account the influence of the phonons in a stochastic manner. This model allows not only to discuss the limiting cases of the completely coherent[40] and completely incoherent[41,42] exciton motion, but also the whole range inbetween.[43,44] A microscopic treatment of the exciton-phonon coupling is given by Haken and Reineker[45] considering the phonons as a heatbath, and by Grover and Silbey[46] taking into account the major part of the exciton-phonon coupling by a canonical transformation. Generalized rate equations for the exciton motion are derived by Kenkre and Knox,[47,48] eliminating the nondiagonal elements of the exciton density matrix by a projection formalism.[49] The relation between these different treatments has been investigated by Kenkre,[50] and some of the theoretical results in connection with the exciton motion have been reviewed by Haken and Reineker[51,52] and by Silbey.[53] Along the same lines as the treatment of the triplet exciton motion proceeded that of its influence on the ESR line shape. The ESR line shape of incoherent excitons may be calculated using the methods of Anderson[54] and of Hudson and McLachlan.[55] The influence of the coherent motion of triplet excitons on their ESR line shape has been investigated by Sternlicht and McConnel,[18] Harris and Fayer,[56] and recently by Berim and Kessel.[57] On the basis of the Haken-Strobl model the influence of the coupled coherent and incoherent exciton motion has been investigated numerically[58] and analytically[59,60] for excitations with spin-$\frac{1}{2}$ moving within molecular pairs.

In this paper the ESR line shape of triplet excitons, moving according to the Haken-Strobl model in a coupled coherent and incoherent manner within a pair of differently oriented molecules (AB pairs), will be discussed as a function of the strengths of the local and nonlocal fluctuation parameters of the model. To that end in Sec. II the Hamiltonian of the model and the equation of motion for the density operator is given. In Sec. III the eigenvalues of the problem and ESR line shapes are represented in dependence of the strengths of the fluctuations parameter. These results are discussed in Sec. IV.

II. HAMILTONIAN OF THE MODEL AND EQUATIONS OF MOTION FOR THE DENSITY OPERATOR

A. The Hamiltonian

The Hamiltonian for our model, describing the dynamics of triplet excitons in a pair system of two differently oriented molecules, consists of two parts. One part describes the electronic degrees of freedom, the other one, the degrees of freedom of the spin. Both parts are coupled owing to the different orientation of the molecules in the pair.

For the excitonic part we use the Hamiltonian of the Haken-Strobl model[37-39] for the coupled coherent and incoherent motion of triplet excitons. The Hamiltonian describing the coherent motion is given by

$$H_{\mathrm{ex},0}=\epsilon_1 b_1^\dagger b_1+\epsilon_2 b_2^\dagger b_2+J(b_1^\dagger b_2+b_2^\dagger b_1)\,. \tag{2.1}$$

$b_i^\dagger$ and b_i are creation and annihilation operators for an electron-hole pair localized at site $i=\{1,2\}$. ϵ_1 and ϵ_2 are the electronic excitation energies of the two noninteracting molecules and J describes the interaction between them; for triplet excitons J is mainly determined by the exchange interaction integral. The coherent motion is disturbed by the phonons, and in the Haken-Strobl model their influence is taken into account in a stochastic manner by letting fluctuate the energy of the excitons and the exchange-interaction integral, resulting in the Hamiltonian

$$H_{\mathrm{ex},1}(t)=\sum_{r,r'} h_{rr'}(t) b_r^\dagger b_{r'}\,. \tag{2.2}$$

Mathematically, it is assumed that the fluctuating quantities $h_{rr'}(t)$ are given by a δ-correlated Gaussian process with disappearing mean value. The nondisappearing correlation functions are given by

$$\begin{aligned}\langle h_{11}(t)h_{11}(t')\rangle &= \langle h_{22}(t)h_{22}(t')\rangle \\ &= 2\gamma_0\delta(t-t')\,,\end{aligned} \tag{2.3}$$

$$\begin{aligned}\langle h_{12}(t)h_{12}(t')\rangle &= \langle h_{12}(t)h_{21}(t')\rangle \\ &= \langle h_{21}(t)h_{12}(t')\rangle \\ &= \langle h_{21}(t)h_{21}(t')\rangle \\ &= 2\gamma_1\delta(t-t')\,.\end{aligned} \tag{2.4}$$

γ_0 is the strength of energy fluctuations (local fluctuations) and γ_1 is the strength of the fluctuations of the interaction integral (nonlocal fluctuations).

The spin Hamiltonian contains the Zeeman energy of a triplet spin $\vec{S}$ in an external magnetic field $\vec{H}$ and fine-structure terms having their origin in the interaction of the two electron spins

forming the triplet state

$$H_{s,0}=g\mu_B\vec{H}\cdot\vec{S}+b_1^\dagger b_1\vec{S}\cdot F^{(1)}\cdot\vec{S}+b_2^\dagger b_2\vec{S}\cdot F^{(2)}\cdot\vec{S}. \tag{2.5}$$

$F^{(1)}$ and $F^{(2)}$ are the fine-structure tensors of the two differently oriented molecules. Introducing the sum and difference of these tensors by

$$M=\tfrac{1}{2}(F^{(1)}+F^{(2)}),\quad D=\tfrac{1}{2}(F^{(1)}-F^{(2)}), \tag{2.6}$$

and the operator Δb for the difference of the excitonic occupation numbers at the two molecules by

$$\Delta b=b_1^\dagger b_1-b_2^\dagger b_2, \tag{2.7}$$

the spin Hamiltonian may be written in the form

$$H_{s,0}=g\mu_B\vec{H}\cdot\vec{S}+\vec{S}\cdot M\cdot\vec{S}+\Delta b\vec{S}\cdot D\cdot\vec{S}. \tag{2.8}$$

This form of the Hamiltonian explicitly shows that the different orientations of the two molecules introduce a coupling between spin and excitonic degrees of freedom.

In the derivation of an equation of motion for the density operator, however, $H_{ex,0}$ and $H_{s,0}$ will be used in the following form:

$$H_{ex,0}=\sum_r \epsilon_r b_r^\dagger b_r+\sum_{r,r'}(1-\delta_{rr'})Jb_r^\dagger b_{r'}, \tag{2.9}$$

$$H_{s,0}=\sum_\sigma H_\sigma S_\sigma+\sum_r\sum_{\sigma,\sigma'} b_r^\dagger b_r S_\sigma S_{\sigma'}F_{\sigma\sigma'}^{(r)}. \tag{2.10}$$

$r,r'=\{1,2\}$ denote the site of the two molecules and $\sigma,\sigma'=\{a,b,c'\}$ denote the crystal axes of the host, in which the pair is imbedded. In (2.10) energies are measured in units of $g\mu_B$. The total Hamiltonian is then given by the sum of the following various parts:

$$H=H_0+H_1(t), \tag{2.11a}$$

$$H_0=H_{ex,0}+H_{s,0}, \tag{2.11b}$$

$$H_1(t)=H_{ex,1}(t). \tag{2.11c}$$

B. Equation of motion

The equation of motion for the density operator is given by

$$\dot{\tilde{\rho}}=-i[H,\tilde{\rho}]=-i[H_0,\tilde{\rho}]-i[H_1(t),\tilde{\rho}]. \tag{2.12}$$

On account of the fluctuating part $H_1(t)$ of the Hamiltonian, $\tilde{\rho}$ still contains fluctuations. Finally, however, for the calculation of expectation values and correlation functions, we are interested in the density operator ρ, which has been averaged over the fluctuations

$$\rho=\langle\tilde{\rho}\rangle=P\tilde{\rho}. \tag{2.13}$$

In this expression we have denoted the time-averaging procedure by the projection operator P, which projects out the fluctuations. Applying this operator, the equation of motion for the density operator becomes

$$\dot{\rho}=-i[H_0,\rho]-iP[H_1(t),\tilde{\rho}]. \tag{2.14}$$

The calculation of the second commutator in this equation is somewhat lengthy, because fluctuations are contained in $H_1(t)$ and in $\tilde{\rho}$. Therefore, this calculation has been carried through in Appendix A with the result given in expression (A1.21). Taking matrix elements between states $|n,s\rangle$, where $n=\{1,2\}$ denotes the site of the excitation and $s=\{a,b,c'\}$ zero-field functions[61] of a triplet spin quantized in the crystal axes system, we have

$$\begin{aligned}-i\{P[H_1(t),\tilde{\rho}]\}_{ns,n's'}=&-2\Gamma\rho_{ns,n's'}\\&+2\delta_{nn'}\sum_{n''}\gamma_{|n''-n|}\rho_{n''s,n''s'}\\&+2(1-\delta_{nn'})\gamma_{|n-n'|}\rho_{n's,ns'},\end{aligned} \tag{2.15}$$

with

$$\Gamma=\gamma_0+\gamma_1. \tag{2.16}$$

The commutators with the two parts of H_0 give the following expressions:

$$-i([H_{ex,0},\rho])_{ns,n's'}=-i\left(\epsilon_n\rho_{ns,n's'}-\epsilon_{n'}\rho_{ns,n's'}+\sum_r(1-\delta_{nr})J\rho_{rs,n's'}-\sum_r(1-\delta_{rn'})J\rho_{ns,rs'}\right), \tag{2.17}$$

$$\begin{aligned}-i([H_{s,0},\rho])_{ns,n's'}=&-\sum_{\sigma s''}H_\sigma(\epsilon_{\sigma ss''}\rho_{ns'',n's'}+\epsilon_{\sigma s's''}\rho_{ns,n's''})-i\Bigg(\sum_{s''(\neq s)}F_{s''s}^{(n)}\rho_{ns,n's'}-\sum_{s''(\neq s)}F_{s''s}^{(n)}\rho_{ns'',n's'}\\&-\sum_{s''(\neq s')}F_{s''s''}^{(n')}\rho_{ns,n's'}+\sum_{s''(\neq s')}F_{s's''}^{(n')}\rho_{ns,n's''}\Bigg).\end{aligned} \tag{2.18}$$

In deriving (2.18) we have used

$$S_\sigma|s'\rangle=i\sum_{s''}\epsilon_{\sigma s's''}|s''\rangle, \tag{2.19}$$

which is valid for the zero-field states introduced above; ϵ_{ijk} is the completely antisymmetric tensor of Levi-Civita.

With (2.15), (2.17), and (2.18), the equation of

motion for the density operator may be written in the following way:

$$\dot{\rho} = \bar{L}\rho . \tag{2.20}$$

[Note that $\bar{L}$ includes a factor $(-i)$ as compared to the Liouville operator of Eq. (A2.2) of Appendix B.] The operator $\bar{L}$ may be written as a 36×36 matrix, if the matrix elements of ρ are arranged in a linear way. To that end we have chosen the following ordering:

$$\rho_1 = \langle 1a|\rho|1a\rangle , \quad \rho_2 = \langle 2a|\rho|2a\rangle , \quad \rho_3 = \langle 1a|\rho|2a\rangle , \quad \rho_4 = \langle 2a|\rho|1a\rangle ; \tag{2.21a}$$

$$\rho_5, \ldots, \rho_8 : \ a \to b , \tag{2.21b}$$

$$\rho_9, \ldots, \rho_{12} : \ b \to c . \tag{2.21c}$$

The last two expressions mean that $\rho_5, \ldots, \rho_8$ and $\rho_9, \ldots, \rho_{12}$ are obtained from $\rho_1, \ldots, \rho_4$ by cyclic permutation of $\{a, b, c\}$:

$$\rho_{13} = \rho_{14}^* = \langle 1a|\rho|1b\rangle , \quad \rho_{15} = \rho_{16}^* = \langle 2a|\rho|2b\rangle , \quad \rho_{17} = \rho_{18}^* = \langle 1a|\rho|2b\rangle , \quad \rho_{19} = \rho_{20}^* = \langle 1b|\rho|2a\rangle ; \tag{2.22a}$$

$$\rho_{21}, \ldots, \rho_{28} : \ a \to b , \ b \to c , \tag{2.22b}$$

$$\rho_{29}, \ldots, \rho_{36} : \ b \to c , \ c \to a . \tag{2.22c}$$

With this notation the matrix $\bar{L}$ has the following structure:

$$\bar{L} = \begin{bmatrix} A & B & C & D \\ -B^\dagger & E & F & G \\ -C^\dagger & -F^\dagger & H & I \\ -D^\dagger & -G^\dagger & -I^\dagger & K \end{bmatrix} ,$$

i.e., it is given by 16 block matrices with the indicated relations, and each of the 16 blocks consists of several 4×4 matrices.

A has nine such 4×4 matrices; only the three on the diagonal, called a, are different from zero and these three are identical and symmetric:

$$A = \begin{bmatrix} a & 0 & 0 \\ 0 & a & 0 \\ 0 & 0 & a \end{bmatrix} ,$$

$$\begin{aligned} &a_{11} = a_{22} = -a_{12} = -a_{34} = -2\gamma_1 , \\ &a_{33} = a_{44}^* = -2\Gamma - i(\epsilon_1 - \epsilon_2) , \\ &a_{13} = a_{14}^* = a_{23}^* = a_{24} = iJ . \end{aligned} \tag{2.23}$$

B consists of six 4×4 matrices, two of which are zero. For the matrices Ba, Bb, Bc, and Bd, only elements different from zero are given:

$$B = \begin{bmatrix} Ba & Bb \\ Bc & Bd \\ 0 & 0 \end{bmatrix} ,$$

$$\begin{aligned} &Ba_{11} = Ba_{12}^* = -H_c - iF_{ab}^{(1)} , \\ &Ba_{23} = Ba_{24}^* = -H_c - iF_{ab}^{(2)} , \\ &Bb_{31} = Bb_{42}^* = -H_c - iF_{ab}^{(2)} , \\ &Bb_{33} = Bb_{44}^* = -H_c + iF_{ab}^{(1)} , \\ &Bc = -Ba , \\ &Bd_{31} = Bd_{42}^* = H_c + iF_{ab}^{(1)} , \\ &Bd_{33} = Bd_{44}^* = H_c - iF_{ab}^{(2)} . \end{aligned} \tag{2.24}$$

Matrices C and D have the following structure:

$$C = \begin{pmatrix} 0 & 0 \\ Ca & Cb \\ Cc & Cd \end{pmatrix} , \quad D = \begin{pmatrix} Dc & Dd \\ 0 & 0 \\ Da & Db \end{pmatrix} .$$

The submatrices of C and D are determined from those of B by cyclic permutation of the indices a, b, c' of $\vec{H}$ and $F^{(i)}$:

$$Ba \to Ca \to Da , \quad Bb \to Cb \to Db , \quad Bc \to Cc \to Dc , \quad Bd \to Cd \to Dd . \tag{2.25}$$

The block matrix E is given by

$$E = \begin{pmatrix} Ea & Eb \\ Ec & Ed \end{pmatrix} ,$$

$$\begin{aligned} &Ea_{11} = Ea_{22}^* = -2\gamma_1 + i(F_{aa}^{(1)} - F_{bb}^{(1)}) , \\ &Ea_{33} = Ea_{44}^* = -2\gamma_1 + i(F_{aa}^{(2)} - F_{bb}^{(2)}) , \\ &Ea_{13} = Ea_{24} = Ea_{31} = Ea_{42} = 2\gamma_1 ; \end{aligned} \tag{2.26}$$

$$\begin{aligned} &Ed_{11} = Ed_{22}^* = -2\Gamma + i(F_{aa}^{(2)} - F_{bb}^{(1)}) - i(\epsilon_1 - \epsilon_2) , \\ &Ed_{33} = Ed_{44}^* = -2\Gamma + i(F_{bb}^{(2)} - F_{aa}^{(1)}) - i(\epsilon_1 - \epsilon_2) , \\ &Ed_{14} = Ed_{23} = Ed_{32} = Ed_{41} = 2\gamma_1 ; \end{aligned} \tag{2.27}$$

$$Eb_{11} = Eb_{14}^* = Eb_{22}^* = Eb_{23} = Eb_{31}^* = Eb_{34} = Eb_{42} = Eb_{43}^* = iJ ; \tag{2.28}$$

$$(Ec)_{ik} = (Eb)_{ki} \quad (i, k = 1, \ldots, 4) . \tag{2.29}$$

The block matrices H and K follow by cyclic permutation of a, b, and c':

$$E \to H \to K , \quad \text{cyclic permutation of } \{a, b, c'\} . \tag{2.30}$$

The remaining blocks are somewhat simpler:

$$F=\begin{pmatrix} Fa & 0 \\ 0 & Fd \end{pmatrix},$$

and the nondisappearing matrix elements of the 4 $\times$ 4 matrices Fa and Fd are given by

$$Fa_{12}=Fa_{21}^{*}=Fd_{13}=Fd_{24}^{*}=H_b+iF_{ac}^{(1)}, \tag{2.31}$$

$$Fa_{34}=Fa_{43}^{*}=Fd_{31}^{*}=Fd_{42}=H_b+iF_{ac}^{(2)}. \tag{2.32}$$

I follows again from cyclic permutation. G has the same structure as F and I, and its nonzero matrix elements may be written in the following way:

$$Ga_{12}=Ga_{21}^{*}=Gd_{31}^{*}=Gd_{42}=-H_a-iF_{bc}^{(1)}, \tag{2.33}$$

$$Ga_{34}=Ga_{43}^{*}=Gd_{13}=Gd_{24}^{*}=-H_a-iF_{bc}^{(2)}. \tag{2.34}$$

With the ansatz $\rho(t)=e^{Rt}\rho$ the differential equation (2.20) for the density operator transforms to a 36-dimensional eigenvalue problem, which will be solved in Sec. III. From the eigensolutions of $\bar{L}$ then the correlation functions describing the ESR line shape may be calculated.

III. SOLUTION OF THE EIGENVALUE PROBLEM AND CALCULATION OF THE ESR LINE SHAPE

A. Parameters of the model

The parameters of our equations are the exchange interaction integral J, the fine-structure tensors $F^{(1)}$ and $F^{(2)}$ of the two differently oriented molecules, the components of the external magnetic field $\vec{H}$, and γ_0 and γ_1, describing the strengths of the local and nonlocal fluctuations, respectively. In our calculations we use values, valid for the naphthalene-h_8 pair embedded in the deuterated host. The exchange interaction integral J is known from optical measurements[29,30]

$$J=1.20\ \text{cm}^{-1}\simeq 1.28\times 10^{4}\ \text{G}. \tag{3.1}$$

We assume that the excitation energies ϵ_1 and ϵ_2 of the isolated molecules are equal, and this value is normalized to zero.

The fine-structure tensors $F^{(1)}$ and $F^{(2)}$ are diagonal in the principle axes system $\{\xi_i,\eta_i,\zeta_i\}$ of the respective molecule and are given by $(i=1,2)$

TABLE I. Direction cosines of the two inequivalent molecules with respect to the crystal axes.

	ξ_1 ξ_2	η_1 η_2	ζ_1 ζ_2
a	$\cos\chi$	$\cos\chi'$	$\cos\chi''$
b	$\pm\cos\psi$	$\pm\cos\psi'$	$\pm\cos\psi''$
c'	$\cos\omega$	$\cos\omega'$	$\cos\omega''$

TABLE II. Angles between molecular axes of molecule 1 and crystal axes.

	ξ_1	η_1	ζ_1
a	115.97°	71.29°	32.87°
b	102.14°	29.33°	116.26°
c'	29.06°	68.26°	71.68°

$$\begin{aligned} F_{\xi_i\xi_i}^{(i)}&=-X=E-\tfrac{1}{3}D,\\ F_{\eta_i\eta_i}^{(i)}&=-Y=-E-\tfrac{1}{3}D,\\ F_{\zeta_i\zeta_i}^{(i)}&=-Z=\tfrac{2}{3}D. \end{aligned} \tag{3.2}$$

The numerical values for the fine-structure parameters are[28]

$$\begin{aligned} D&=1063.3\ \text{G}\simeq 9.9387\times 10^{-2}\ \text{cm}^{-1},\\ E&=-164.7\ \text{G}\simeq -1.534\times 10^{-2}\ \text{cm}^{-1}. \end{aligned} \tag{3.3}$$

[The D used here should not be mixed up with that of (2.6), which is the difference of the fine-structure tensors.] The orientations of the principle axes systems $\{\xi_i,\eta_i,\zeta_i\}$ of both molecules with respect to the crystal axes system $\{a,b,c'\}$ are determined by the direction cosines of Table I and the angles of Table II.[62] The strength of the magnetic field is assumed to be

$$|\vec{H}|=4000\ \text{G}\simeq 0.373\,88\ \text{cm}^{-1}. \tag{3.4}$$

In all subsequent calculations $\vec{H}$ is oriented in the y_p-z_p plane of an axes system $\{x_p,y_p,z_p\}$ and forms an angle of $+60°$ with the y_p axis. The system $\{x_p,y_p,z_p\}$ is defined by the tensor M of (2.6) being diagonal. In naphthalene crystals the y_p axis coincides with the b axis of the crystal; the angle between the $+z_p$ axis and the $+a$ axis is $+22.4°$.[63,64]

In Sec. III B the eigenvalues of the matrix $\bar{L}$ and ESR line shapes are pictured as a function of the strengths of the fluctuation parameters γ_0 and γ_1.

B. Eigenvalues of the matrix $\bar{L}$

In order to solve the eigenvalue problem of the density matrix ρ,

$$\bar{L}\rho^{i}=R_i\rho^{i}, \tag{3.5}$$

the non-Hermitean matrix $\bar{L}$ has been transformed into a nonsymmetric real form by a unitary transformation. In the computer evaluation of this eigenvalue problem a modified version of a program of Grad and Brebner[65] has been used. The numerical calculation[66] proceeds in three steps. First, the real nonsymmetric matrix is transformed to upper Hessenberg form by similarity transformations. In the second step, the eigenvalues are calculated by an iteration procedure called "Q-R double-step method," a modification

TABLE III. Energy eigenvalues E_i of the Schrödinger equation (3.5) describing the AB pair in the unit cell of naphthalene crystals and transition energies ΔE for $\Delta m = 1$ and $\Delta m = 2$ ESR transitions.

E_i (G)	$\Delta E(\Delta m = 1)$ (G)	$\Delta E(\Delta m = 2)$ (G)
E_1: 17015.00	4596.85	8037.11
E_3: 12418.15	3440.26	
E_5: 8977.89		
E_2: −8590.49	4601.75	8037.83
E_4: −13192.24	3436.08	
E_6: −16628.32		

of the "Q-R method," which works better for matrices with complex eigenvalues.

The 36-dimensional eigenvalue problem results in 36, generally complex, eigenvalues R_i. The real and imaginary parts of these eigenvalues have been pictured separately in the following figures as a function of the strength of the local fluctuations γ_0 for a fixed value of the nonlocal fluctuations γ_1 and as a function of γ_1 for a fixed value of γ_0. The real and imaginary parts belonging to the same eigenvalue R_i are denoted by the same number. Between six and 12 of the 36 eigenvalues are purely real, and the remaining ones occur in complex conjugate pairs. Therefore we have between 21 and 24 different real parts. In the second case the three additional real parts are denoted by 4′, 5′, and 6′. The eigenvalue for the stationary eigenstate is always denoted by 21, i.e., $R_{21} = 0$. Because the complex eigenvalues occur in complex conjugate pairs, only half of the imaginary parts has been shown, and their total number is obtained by reflection of the figures at the γ axis. Finally, we should mention that the eigenvalues R represent the total exponent; therefore, their real parts describe relaxations and their imaginary parts, oscillations. The relation between R_i and the eigenvalues $\tilde{R}_i$ introduced in Appendix B is given by $R_i = -i\tilde{R}_i$.

TABLE IV. Energy eigenvalues E_{Ai} and E_{Bi} of the Schrödinger equation (3.5) for the isolated A and B molecules ($J = 0$) in the unit cell of the naphthalene crystal.

E (cm^{-1})	$\Delta E(\Delta m = 1)$ (cm^{-1})	$\Delta E(\Delta m = 2)$ (cm^{-1})
E_{A1}: 0.3818	0.3884	0.7575
E_{A2}: −0.0066	0.3686	
E_{A3}: −0.3752		
E_{B1}: 0.4071	0.4728	0.7485
E_{B2}: −0.0657	0.2757	
E_{B3}: −0.3414		

For comparison with these eigenvalues of the density matrix equation, in Table III the energy eigenvalues E_i of the Schrödinger equation

$$(H_{ex,0} + H_{s,0})\psi_i = E_i\psi_i\,, \tag{3.6}$$

describing the case of the coherent exciton motion[64,67] with $\gamma_0 = \gamma_1 = 0$, for the upper (E_1, E_3, E_5) and lower (E_2, E_4, E_6) Davydov components are given in the first column. The second column gives energy differences ΔE for $\Delta m = 1$ ESR transitions in the upper and lower Davydov components, and the third one, transition energies with $\Delta m = 2$. Table IV gives the energy eigenvalues E_{Ai} and E_{Bi} of (3.6) for $J = 0$, i.e., the energy eigenvalues of the isolated A and B molecules in the unit cell. In this table energies are measured in units of cm^{-1} (1 cm^{-1} $\simeq 1.06986 \times 10^4$ G).

Figures 1(a) and 1(b) show the imaginary and real parts of the eigenvalues R_i for $\gamma_1 = 10^{-5}$ G as a function of γ_0. Note that in Fig. 1(a), on the vertical axis, several different scales are used. The comparison of Im(R) for small values of γ_0 (<0.3 G) with the values of Table III shows that Im(R_i) with $i = 1$—6 and 13—15 coincides with energy differences between the upper (E_1, E_3, E_5) and lower (E_2, E_4, E_6) Davydov components. Im(R_7) and Im(R_8) describe $\Delta m = 2$ transitions within the lower and upper Davydov components, respectively. Again from Table III we conclude that Im(R_i) with $i = 9$ and 12 and with $i = 10$ and 11 correspond to ESR transitions with $\Delta m = 1$ between energy levels within the lower and upper Davydov components, respectively. With increasing values of γ_0 up to $\gamma_0 = 3$ G, the imaginary parts of the eigenvalues describing transitions between levels of the upper and the lower Davydov components remain constant. The imaginary parts of the eigenvalues R_i describing corresponding ESR transitions between levels within the upper and lower Davydov components, however, move together with increasing γ_0, and for large enough values of γ_0 they finally coalesce. For eigenvalues 7 and 8 this happens at $\gamma_0 \approx 0.3$ G, for 9 and 10 at $\gamma_0 \approx 2.4$ G, and for 11 and 12 at $\gamma_0 \approx 2.1$ G.

The real parts of the eigenvalues, except those ones corresponding to ESR transitions, increase with increasing γ_0. The real parts of the eigenvalues 7 and 8, 11 and 12, and 9 and 10, however, split into two different values for the same values of γ_0, for which their imaginary parts coincide. One of these real parts of each pair increases (8, 10, 12) with increasing γ_0, the other one first decreases (7, 9, 11) and then increases again.

This increasing behavior of all real parts of the eigenvalues continues up to $\gamma_0 \approx 2.4$ cm^{-1} ($\simeq$ 25 000 G). This may be seen in Fig. 2(c), where the real

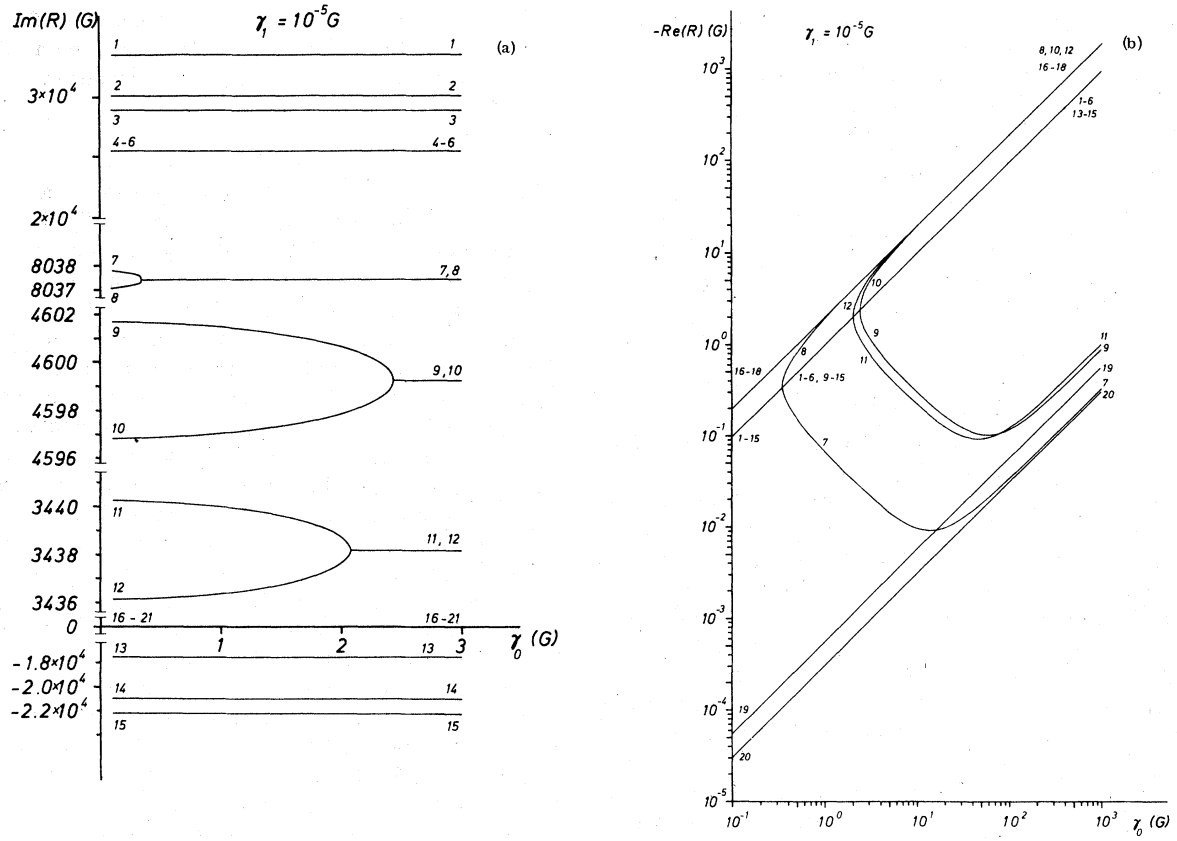

FIG. 1. (a) Imaginary parts of the eigenvalues R_i of the density-matrix equation for γ_0 between 0.1 and 3 G and for $\gamma_1 = 10^{-5}$ G. From the total number of 36 eigenvalues, six are purely real (16–21), the remaining 30 occur in complex conjugate pairs. Only 15 of the 30 different imaginary parts are shown, the second half is obtained by reflection at the γ_0 axis. (Exchange interaction integral: $J = 12\,800$ G, fine structure parameters: $D = 1063.3$ G, $E = -164.7$ G; strength of the magnetic field, which lies completely within the y_p-z_p plane: $|\vec{H}| = 4000$ G; angle between $\vec{H}$ and the y_p-z_p plane: $|\vec{H}| = 4000$ G; angle between $\vec{H}$ and the y_p axis: $\alpha = +60°$). (b) Real parts of the eigenvalues R_i for values of γ_0 between 0.1 and 1000 G and for $\gamma_1 = 10^{-5}$ G. The other parameters are the same as in (a).

parts of the eigenvalues have been pictured for $\gamma_1 = 10^{-4}$ cm^{-1} again as a function of γ_0. (Note that we have now changed to units of cm^{-1}.) For $\gamma_0 \approx 2.4$ cm^{-1} the real parts of the eigenvalues 1-6, 4′-6′, and 13-15 split into two groups 1-3, 4′-6′ and 4-6, 13-15, the first of which increases with increasing γ_0; the second one decreases. From what we have learned in the discussion of Figs. 1(a) and 1(b), we now expect that at this value of γ_0 the imaginary parts of these eigenvalues coincide. This behavior shows Fig. 2(a), where the imaginary parts of the pairs of eigenvalues 1 and 13, 2 and 14, 3 and 15, 4-6 and 4′-6′ coalesce. (The imaginary parts of 4′-6′ have not been pictured according to our convention above, because these eigenvalues are complex conjugate to 4-6.)

For γ_0 increasing further, now the real parts of the eigenvalues R_{11} and R_{15}, R_9 and R_{14} coalesce ($\gamma_0 \approx 30$ cm^{-1}) and we now expect, the other way round, the imaginary parts to split. This splitting shows Fig. 2(b), where the imaginary parts are shown for values of γ_0 up to 100 cm^{-1}. When γ_0 increases further, the imaginary parts of the eigenvalues split step by step, and for very large values of γ_0 we again arrive at 15 pairs of complex conjugate eigenvalues and six purely real ones. The dashed lines give the eigenvalues for $\gamma_0 = 10\,000$ cm^{-1}. The comparison with Table IV shows that the imaginary parts of the eigenvalues R_i now describe the differences in the energy eigenvalues of the two differently oriented non-interacting naphthalene molecules in the unit cell of the deuterated crystal. [The growing together of the real parts of the eigenvalues, accompanying the splitting of the corresponding imaginary parts, cannot be observed in all cases on account of the scale used in Fig. 2(c).] Furthermore, we conclude that R_9 and R_{15} describe $\Delta m = 1$ ESR tran-

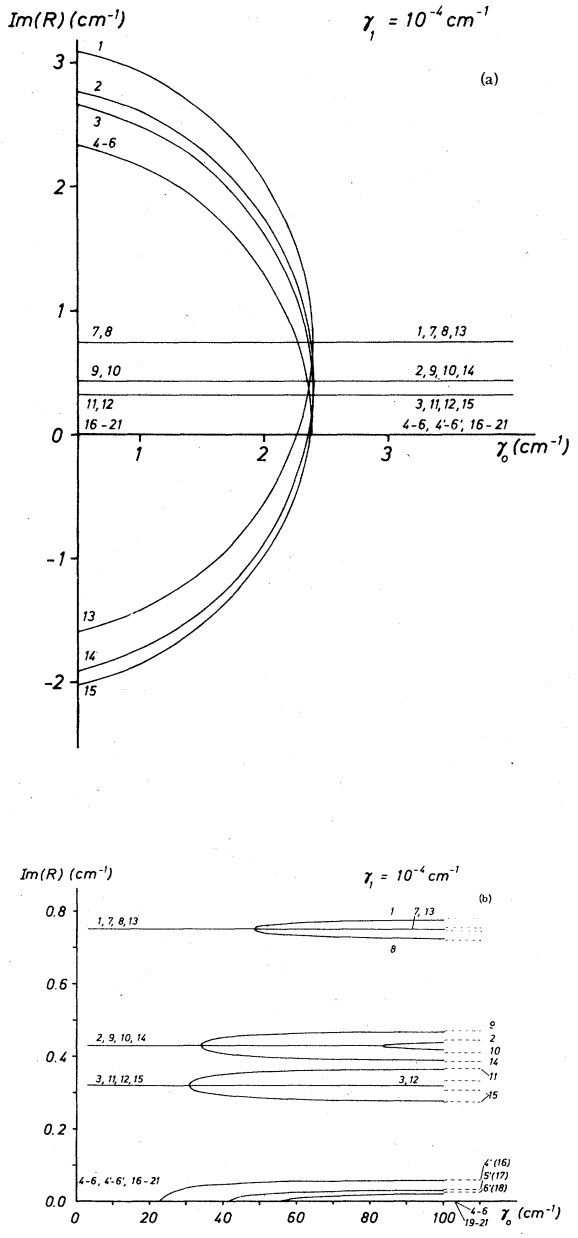

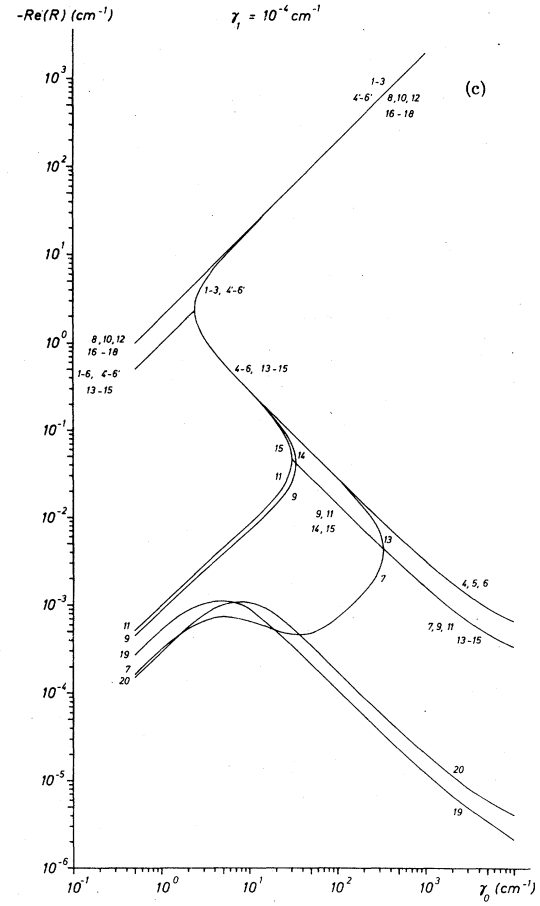

FIG. 2. (a) Imaginary parts of the eigenvalues R_i for values of γ_0 between 0.5 and 4 cm^{-1} and for $\gamma_1 = 10^{-4}$ cm^{-1}. [Exchange interaction integral $J = 1.20$ cm^{-1}; fine-structure parameters $D = 9.9387 \times 10^{-2}$ cm^{-1}, $E = -1.535 \times 10^{-2}$ cm^{-1}; strength of the magnetic field $|\vec{H}| = 0.37388$ cm^{-1}; orientation of $\vec{H}$ as in Fig. 1(a).] (b) Imaginary parts of the eigenvalues R_i for γ_0 between 3 and 100 cm^{-1} and for $\gamma_1 = 10^{-4}$ cm^{-1}. The dashed lines give the values for $\gamma_0 = 10^4$ cm^{-1}. The other parameters are the same as in (a). (c) Real parts of the eigenvalues R_i for γ_0 between 5 and 10^4 cm^{-1} and for $\gamma_1 = 10^{-4}$ cm^{-1}. The other parameters are the same as in (a).

sitions at the B molecule and R_{11} and R_{14} at the A molecule.

The following figures show the eigenvalues of the density matrix equation for fixed values of the strength of the local fluctuations γ_0 as a function of γ_1. In Figs. 3(a) and 3(b), the value of γ_0 is 0.1 G. The comparison if Figs. 1(a) and 3(a) shows that the imaginary parts of the eigenvalues do not change up to $\gamma_1 \approx 10^3$ G. When γ_1 increases further, the imaginary parts of the eigenvalues R_i ($i = 1, \ldots, 6; 13, \ldots, 15$) describing energy differences between the levels of different Davydov components remain unchanged, whereas the imaginary parts of the pairs of eigenvalues denoted by 7 and 8, 9 and 10, and 11 and 12, describing ESR transitions move together. From Fig. 3(b) we see that the real parts of the eigenvalues, describing energy differences between levels of different Davydov components increase continuously with increasing γ_1. The real parts of the eigenvalues R_7 to R_{12} and the purely real eigenvalues R_{16}-R_{20} first increase up to values of γ_1 between 10^3 and 10^4 G and then decrease with γ_1 increasing further. A closer inspection shows that the real parts

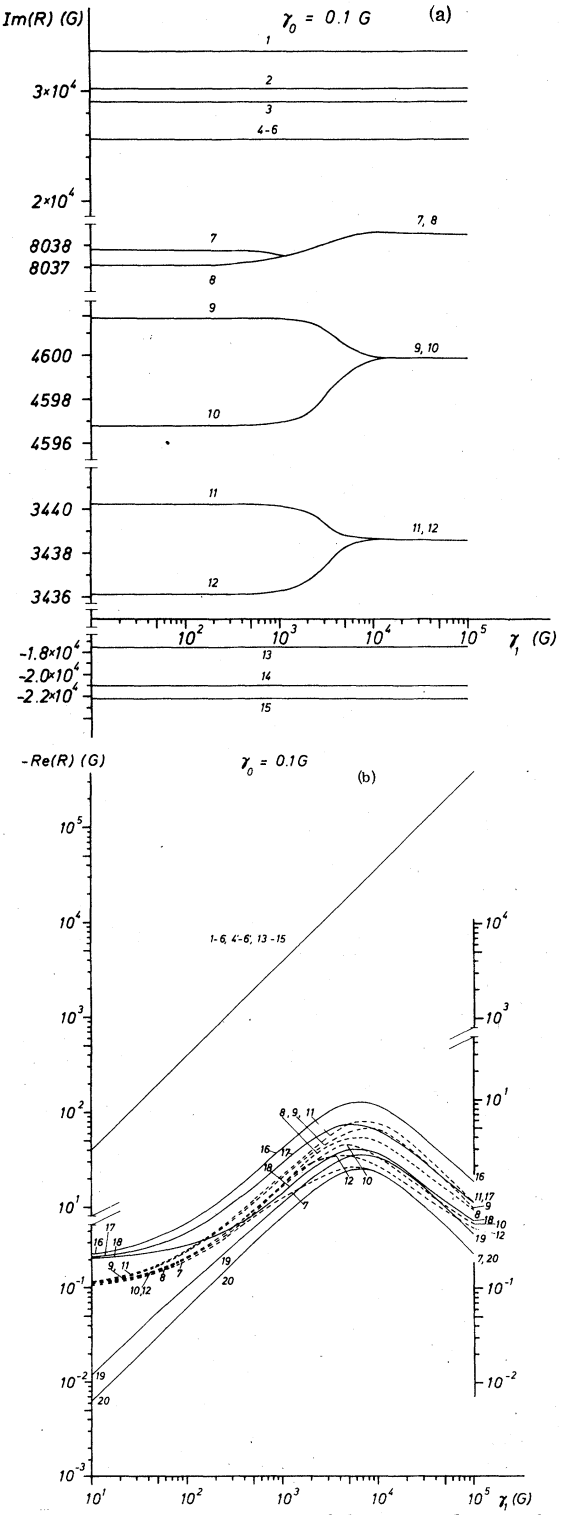

FIG. 3. (a) Imaginary parts of the eigenvalues R_i for values of γ_1 between 10 and 10^5 G and for $\gamma_0 = 0.1$ G. The other parameters are the same as in Fig. 1(a). (b) Real parts of the eigenvalues R_i for values of γ_1 between 10 and 10^5 G and for $\gamma_0 = 0.1$ G. The other parameters are the same as in Fig. 1(a).

of the eigenvalues R_7 to R_{12} separate themselves at those values of γ_1, at which the corresponding imaginary parts coincide.

Figures 4(a) and 4(b) give the imaginary and real parts of the eigenvalues for $\gamma_0 = 0.1$ cm^{-1}. Figure 4(a) shows that the imaginary parts for this value of γ_0 are nearly independent on γ_1. The real parts of the complex eigenvalues R_8, R_{10}, and R_{12} and the purely real eigenvalues R_{16} to R_{18} are also independent on γ_1. The real parts of the complex eigenvalues R_7, R_9, and R_{11} and the real eigenvalues R_{19} and R_{20} first increase with increasing γ_1; for $\gamma_1 > 0.5$ cm^{-1} they decrease again. The real parts of the complex eigenvalues R_i ($i = 1$-6; 4'-6'; 13-15), whose imaginary parts describe, for small values of γ_0 and γ_1, transitions between the levels of different Davydov components, continuously increase with γ_1 becoming larger.

In Figs. 5(a) and 5(b) we have the imaginary and real parts of the eigenvalues for $\gamma_0 = 20$ cm^{-1}. The comparison with the imaginary parts of the eigenvalues of Fig. 2(b) for $\gamma_0 = 20$ cm^{-1} shows that Im(R_i) for $i = 1$, 7, 8, and 13, for $i = 2$, 9, 10, and 14, and $i = 3$, 11, 12, and 15 is unchanged when γ_1 increases. The imaginary parts of the eigenvalues 4' and 16 and of 5' and 17 split off from zero for $\gamma_1 \approx 10^{-2}$ cm^{-1}. This behavior may be compared with that of the imaginary parts 4' and 16 and 5' and 17 in Fig. 2(b) for increasing values of γ_0. In contrast to the behavior of these eigenvalues for increasing γ_0, in the case of increasing γ_1 their imaginary parts again decrease to zero for $\gamma_1 \approx 0.1$ cm^{-1}. Starting from the real parts of the eigenvalues for $\gamma_0 = 20$ cm^{-1} in Fig. 2(c), we see from Fig. 5(b) that the real parts of the eigenvalues 1 to 3, 4' to 6', 8, 10, 12, and 16 to 18 are practically independent of γ_1 in contrast to their strong dependence on γ_0. The remaining real parts (7, 9, 11, 19, and 20) decrease with increasing γ_1.

Figures 6(a) and 6(b) show the eigenvalues for $\gamma_0 = 1000$ cm^{-1}. For small values of the nonlocal fluctuations ($\gamma_1 \approx 10^{-3}$ cm^{-1}) in Fig. 6(a) we have the 15 different imaginary parts of the eigenvalues shown in Fig. 2(b) for large values of γ_0. In connection with the discussion of that figure we remarked that these imaginary parts describe the differences between the energy levels of the noninteracting molecules sitting substitutionally in the unit cell of naphthalene. With increasing values of γ_1 these eigenvalues move together in pairs, and for very high values of γ_1 we remain with only three imaginary parts, which are different from zero. In Fig. 6(b) we may again observe that for those values of γ_1, where two imaginary parts finally coincide, the real parts begin to split. One of the two real parts of such a pair increases, the

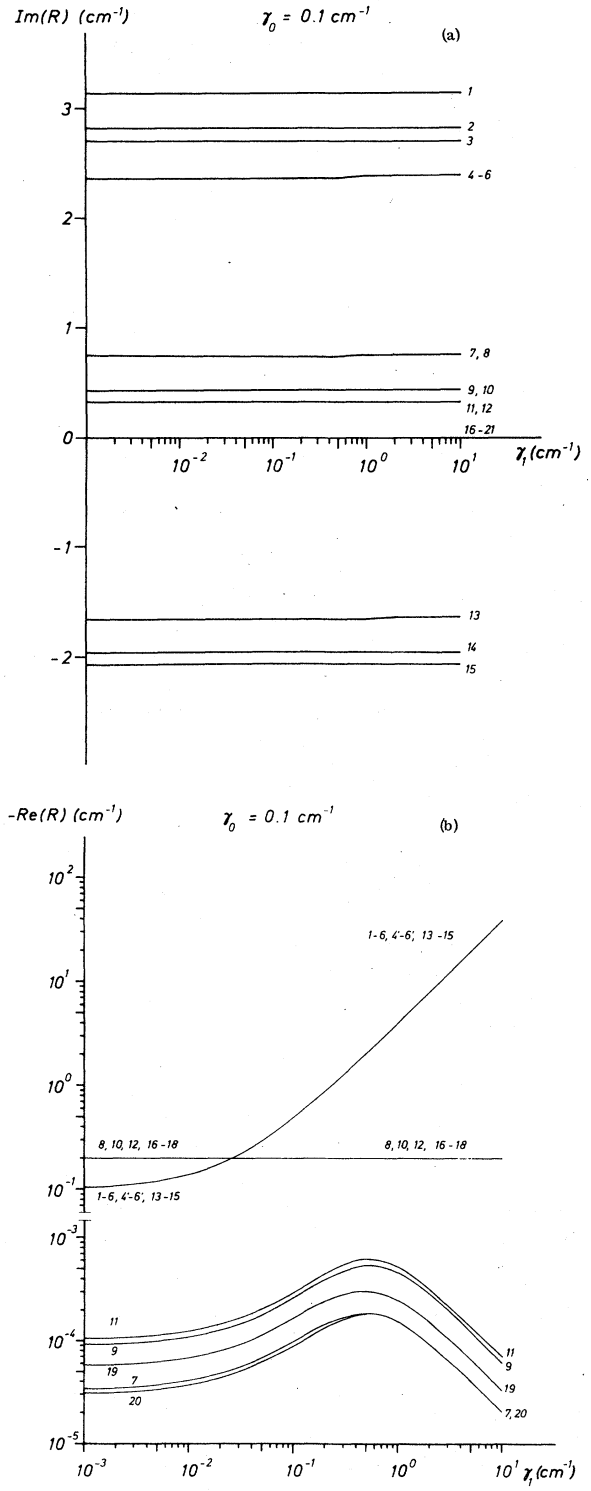

FIG. 4. (a) Imaginary parts of the eigenvalues R_i for values of γ_1 between 10^{-3} and 10 cm^{-1} and for $\gamma_0 = 0.1$ cm^{-1}. The other parameters are the same as in Fig. 2(a). (b) Real parts of the eigenvalues R_i for values of γ_1 between 10^{-3} and 10 cm^{-1} and for $\gamma_0 = 0.1$ cm^{-1}. The other parameters are the same as in Fig. 2(a).

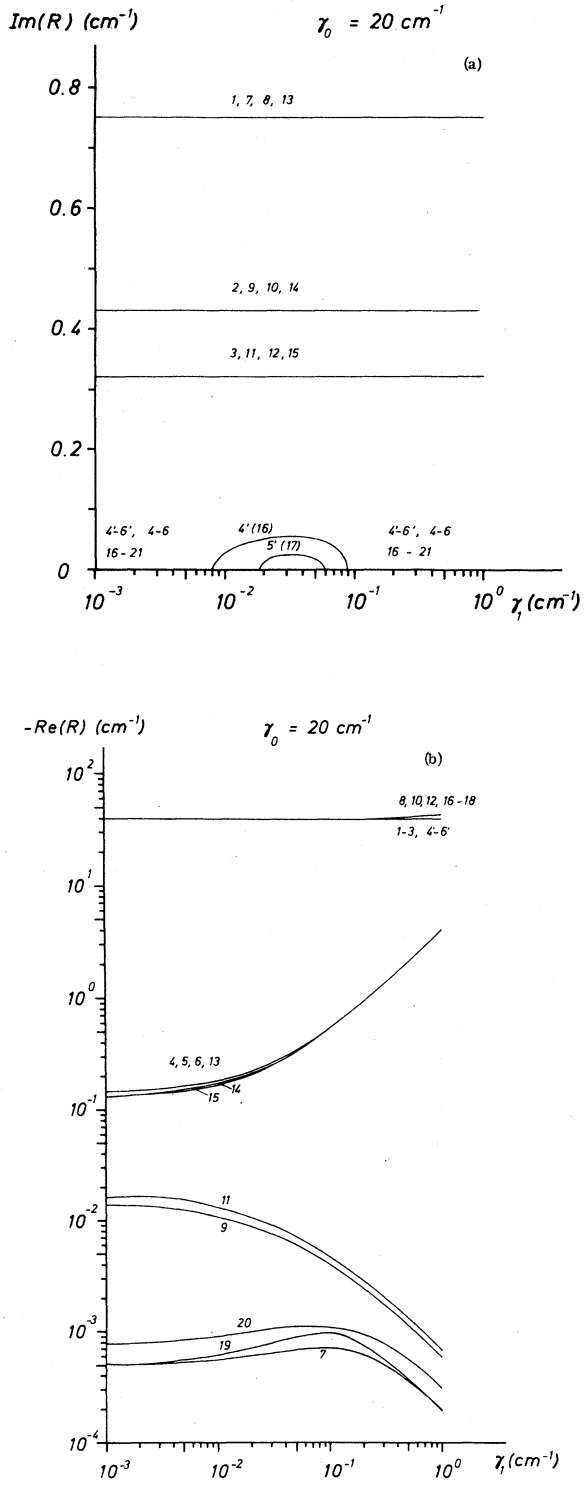

FIG. 5. (a) Imaginary parts of the eigenvalues R_i for values of γ_1 between 10^{-3} and 1 cm^{-1} and for $\gamma_0 = 20$ cm^{-1}. The other parameters are the same as in Fig. 2(a). (b) Real parts of the eigenvalues R_i for values of γ_1 between 10^{-3} and 1 cm^{-1} and for $\gamma_0 = 20$ cm^{-1}. The other parameters are the same as in Fig. 2(a).

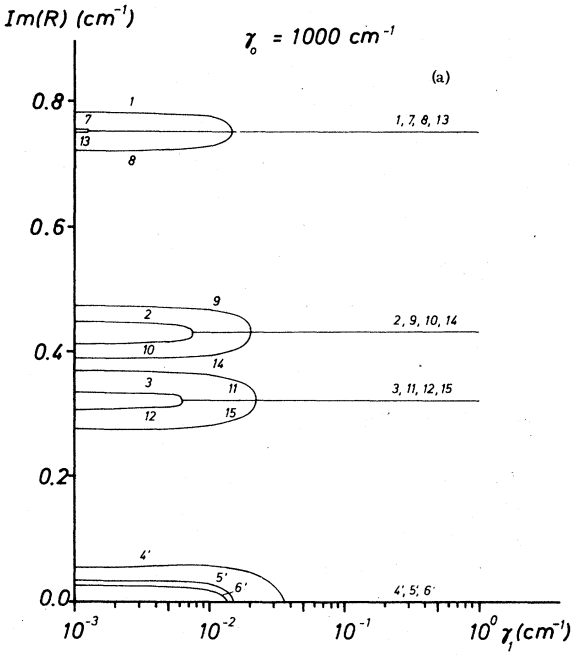

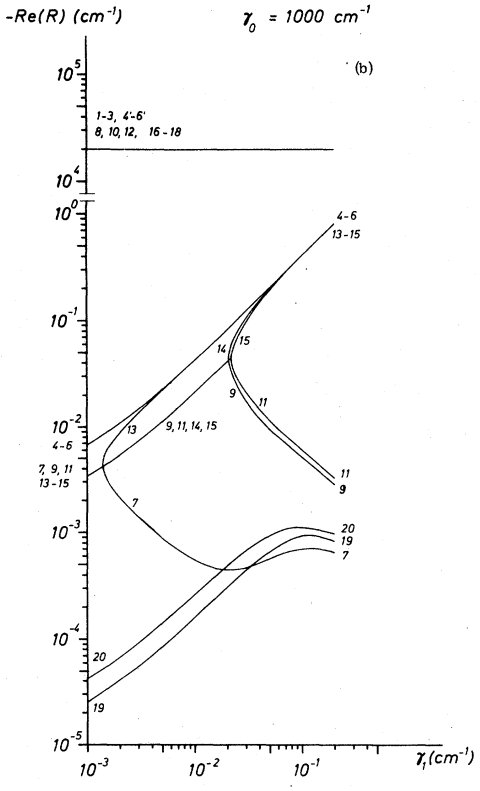

FIG. 6. (a) Imaginary parts of the eigenvalues R_i for values of γ_1 between 10^{-3} and 1 cm^{-1} and for $\gamma_0 = 1000$ cm^{-1}. The other parameters are the same as in Fig. 2(a). (b) Real parts of the eigenvalues R_i for values of γ_1 between 10^{-3} and 1 cm^{-1} and for $\gamma_0 = 1000$ cm^{-1}. The other parameters are the same as in Fig. 2(a).

other decreases. In Sec. IIIC, in which the ESR line shapes are considered, we shall observe that these decreasing real parts are responsible for their widths.

C. ESR line shapes

In linear approximation in Appendix B the response of an observable B on a perturbation A has been calculated for systems, whose time development is determined by a non-Hermitean Liouville operator. In the high-temperature approximation,[68] which is consistent within the Haken-Strobl model, the ESR line shape is determined by the imaginary part of the magnetic susceptibility according to (A2.18):

$$\chi''(\omega) = \beta\omega \int_0^\infty d\tau (M_x, e^{\bar{L}\tau} M_x) \cos\omega\tau \,, \tag{3.7}$$

where

$$(A, B) \equiv \mathrm{Tr}(A^\dagger B) \,. \tag{3.8}$$

In writing (3.7) it was assumed that the microwave field is parallel to the x axis and perpendicular to the magnetic high field. Using the eigenvalues R_i and eigenvectors ρ^i of the operator $\bar{L}$ as well as the eigenvectors η^i of the adjoint operator $\bar{L}^\dagger$, we have, from (A2.20),

$$\chi'' = \frac{i}{N} \sum_j (\eta^s, M_x \rho^j)(\eta^j, M_x \rho^s) \left(\frac{\omega}{\omega + \tilde{R}_j} \quad \frac{\omega}{\omega - \tilde{R}_j} \right), \tag{3.9}$$

$$\tilde{R}_j = iR_j = \tilde{\omega}_j - i\tilde{\gamma}_j \,. \tag{3.10}$$

ρ^s and η^s are the stationary solutions of $\bar{L}$. The normalization constant N is determined from

$$\int_0^\infty \chi''(\omega)\, d\omega = 1 \,. \tag{3.11}$$

With the help of the eigensolutions of the density matrix equation it may be calculated according to (A2.29):

$$N = \sum_j (\eta^s, M_x \rho^j)(\eta^j, M_x \rho^s)(-i\tilde{R}_j) \times \left[-\ln(\tilde{\omega}_j^2 + \tilde{\gamma}_j^2) + 2i \arctan\left(\frac{\tilde{\gamma}_j}{\tilde{\omega}_j} \right) \right]. \tag{3.12}$$

ESR line shapes calculated in this way are pictured in Figs. 7 to 15. In all figures the exchange interaction integral, the fine structure parameters and the strength and orientation of the static magnetic field have the values of Sec. IIIA. As in the discussion of the eigenvalues in each figure either the strength of the local fluctuations γ_0 or the strength of the nonlocal fluctuations γ_1 is varied, while the other parameter is fixed.

Figure 7 gives the ESR line shape for fixed $\gamma_1 = 10^{-5}$ G and for values of γ_0 between 0.1 and 1000 G (≈ 0.1 cm^{-1}). On account of the large ω scale in this figure only the lines corresponding to transitions between levels E_3 and E_5 and between E_4 and E_6 (compare Table III) in the upper and lower Davydov component are pictured. The positions of these two lines is given by the imaginary parts denoted by 11 and 12 in Fig. 1(a). The positions of the ESR lines corresponding to transitions between E_1 and E_3 and between E_2 and E_4 are determined by the imaginary parts denoted by 10 and 9, respectively. With increasing values of γ_0 the lines of Fig. 7 broaden and move together. For values of $\gamma_0 > 2$ G, we have only a single line which narrows with increasing γ_0. This behavior of the ESR line is reflected in Figs. 1(a) and 1(b) for the eigenvalues. With increasing values of γ_0 the two imaginary parts 11 and 12 move together, and for $\gamma_0 > 2$ G, they coalesce into a single value in the middle between the original ones. For the same value of γ_0 the real parts 11 and 12 split, and it is obvious that the narrowing of the ESR line is described by the real part of eigenvalue 11. For $\gamma_0 > 50$ G, this real part increases again, which results in the broadening of the ESR line for $\gamma_0 > 50$ G. The position of the line, however, remains unchanged.

A completely analogous behavior shows the ESR lines determined by the eigenvalues R_9 and R_{10} and stemming from transitions between E_2 and E_4 and between E_1 and E_3, respectively. These ESR transitions have also been taken into account in Fig. 8, showing the ESR spectrum for larger values of γ_0. The position of the line shown in Fig. 7 is at $\omega \approx 0.32$ cm^{-1}. With increasing γ_0 the real parts of the eigenvalues R_9 and R_{11} increase [see Fig. 2(c)] giving rise to the broadening of the ESR lines in Fig. 8. At $\gamma_0 \approx 30$ cm^{-1}, these real parts coalesce with those of the eigenvalues R_{14} and R_{15}, and the imaginary parts of R_9, R_{14} and R_{11} and R_{15}

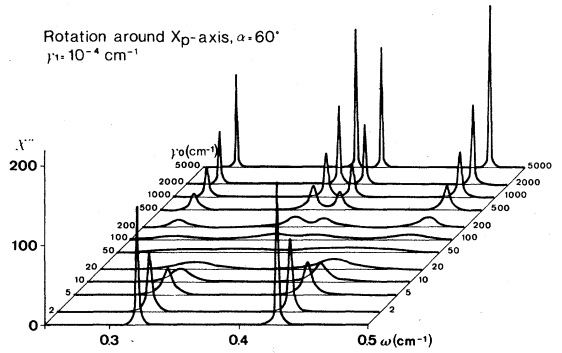

FIG. 8. ESR line shape for values of γ_0 between 1 and 5000 cm^{-1} and for $\gamma_1 = 10^{-4}$ cm^{-1}. The other parameters are the same as in Fig. 2(a).

split [see Fig. 2(b)]. When γ_0 increases further the real parts of these eigenvalues decrease. For large enough values of γ_0 we arrive at four narrow ESR lines whose positions are determined by Table IV, and which describe $\Delta m = 1$ ESR transitions in the noninteracting A and B molecules.

The following figures give ESR line shapes when γ_0 is held fixed and γ_1 varies. In Fig. 9 we have $\gamma_0 = 0.1$ G. For small values of γ_1 we again have the narrow ESR lines just pictured in Fig. 7 and determined by R_{11} and R_{12} of Fig. 1(a). These lines broaden with increasing γ_1 and coalesce into a single line for $\gamma_1 \approx 5000$ G ($\simeq 0.5$ cm^{-1}). For still larger values of γ_1 a narrowing starts. The corresponding behavior of the imaginary and real parts of the eigenvalues is shown in Figs. 3(a) and 3(b); for $\gamma_1 > 5000$ G, the imaginary parts of R_{11} and R_{12} have moved together, and their real parts decrease. The behavior of the lines determined by R_9 and R_{11} is analogous.

In Fig. 10 for $\gamma_0 = 1$ G, the ESR lines for small values of γ_1 are much broader than the corresponding lines of Fig. 9 because of the larger value of γ_0. From the comparison with Fig. 7 this broader initial line is expected. When γ_1 in-

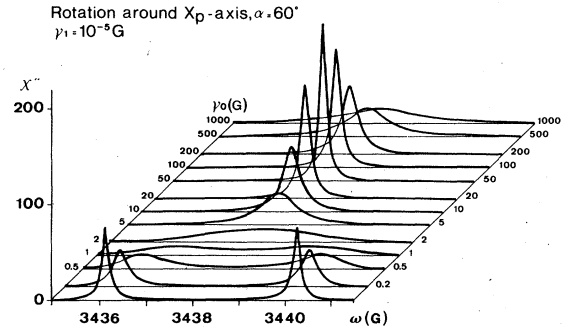

FIG. 7. ESR line shape for values of γ_0 between 0.1 and 1000 G and for $\gamma_1 = 10^{-5}$ G. The other parameters are the same as in Fig. 1(a).

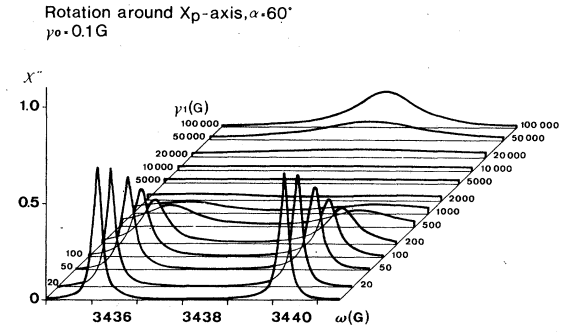

FIG. 9. ESR line shape for values of γ_1 between 10 and 10^5 G and for $\gamma_0 = 0.1$ G. The other parameters are the same as in Fig. 1(a).

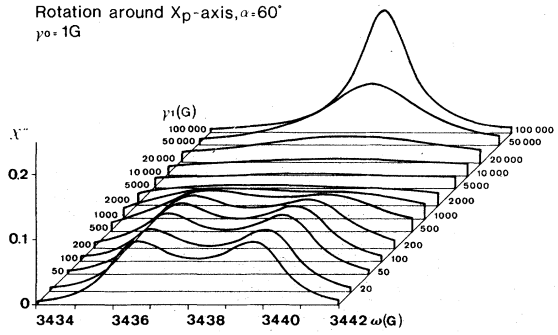

FIG. 10. ESR line shape for values of γ_1 between 10 and 10^5 G and for $\gamma_0 = 1$ G. The other parameters are the same as in Fig. 1(a).

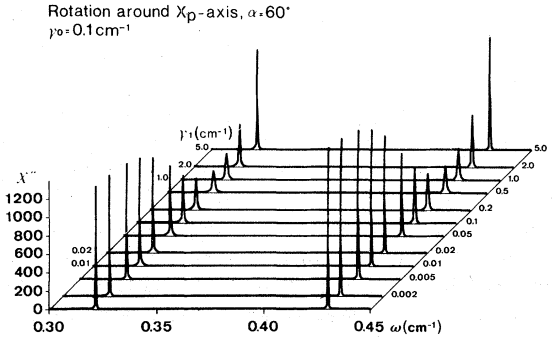

FIG. 12. ESR line shape for values of γ_1 between 10^{-3} and 5 cm^{-1} and for $\gamma_0 = 0.1$ cm^{-1}. The other parameters are the same as in Fig. 2(a).

creases, the lines become first broader and then smaller for $\gamma_1 > 5000$ G.

For $\gamma_0 = 1000$ G (≈ 0.1 cm^{-1}) in Fig. 11 we have for small values of γ_1 a single ESR line, stemming from the transitions between the energy levels E_3 and E_5 and between E_4 and E_6. This line may be compared with that in Fig. 7 for $\gamma_0 = 1000$ G. With increasing nonlocal fluctuations the line broadens up to $\gamma_1 = 5000$ G; for still larger values of γ_1 the narrowing sets in. From Fig. 4(a) we see that the imaginary part of the eigenvalue R_9 and thus the line position are independent of γ_1, whereas the real part of this eigenvalue in Fig. 4(b) first increases and then decreases.

In Fig. 12, in addition to the line stemming from the transitions between E_3 and E_5 and between E_4 and E_6, the line originating in the transitions between E_1 and E_3 and between E_2 and E_4 also are shown. The width of both lines first increases up to $\gamma_1 = 0.5$ cm^{-1} and then decreases. The eigenvalues belonging to this case are given in Figs. 4(a) and 4(b).

The ESR spectrum for $\gamma_0 = 20$ cm^{-1} shows also only two lines (Fig. 13), which are relatively broad for small values of γ_1. With increasing values of γ_1 the widths of the two lines become smaller. The eigenvalues R_9 and R_{11} in Figs. 5(a) and 5(b) describe this situation.

Additional structure shows the ESR spectrum in Fig. 14 for $\gamma_0 = 100$ cm^{-1}. From Fig. 8 we know that for this value of γ_0 and small values of γ_1, four ESR lines begin to appear. This may also be seen from Fig. 2(b) for the imaginary parts of the eigenvalues. With increasing values of γ_1, the four lines become broader, merge into two lines, and finally the two lines become smaller.

This behavior is still more distinct in the spectrum of Fig. 15. For $\gamma_0 = 1000$ cm^{-1} and small values of γ_1 we have four narrow ESR lines, a situation which is also pictured in Fig. 8. The position of these lines is determined by the differences of the energy eigenvalues of the noninteracting molecules in the unit cell. When γ_1 increases these lines become broader until for $\gamma_1 \approx 0.02$ cm^{-1} they merge by pairs into two lines which narrow when γ_1 increases further. This behavior is reflected in the γ_1 dependence of the imaginary and real parts of the eigenvalues in Figs. 6(a) and 6(b). For $\gamma_1 \approx 0.02$ cm^{-1} the imaginary parts of R_9 and R_{14} and those of R_{11} and R_{15} merge into two values

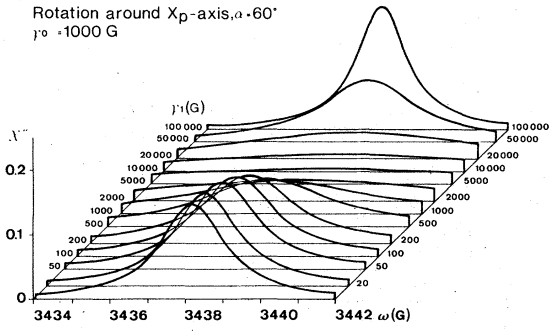

FIG. 11. ESR line shape for values of γ_1 between 10 and 10^5 G and for $\gamma_0 = 1000$ G. The other parameters are the same as inFig. 1(a).

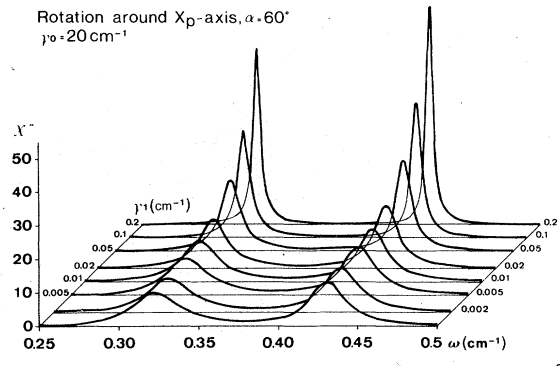

FIG. 13. ESR line shape for values of γ_1 between 10^{-3} and 0.2 cm^{-1} and for $\gamma_0 = 20$ cm^{-1}. The other parameters are the same as in Fig. 2(a).

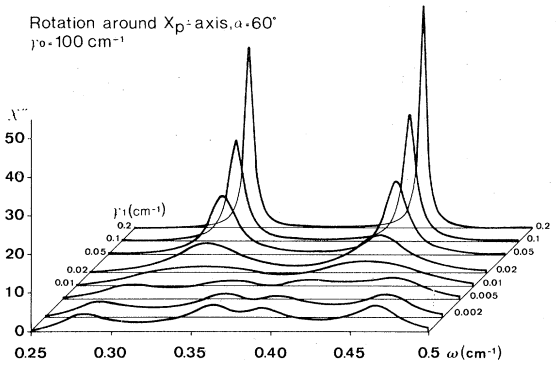

FIG. 14. ESR line shapes for values of γ_1 between 10^{-3} and 0.2 cm^{-1} and for $\gamma_0 = 100\ cm^{-1}$. The other parameters are the same as in Fig. 2(a).

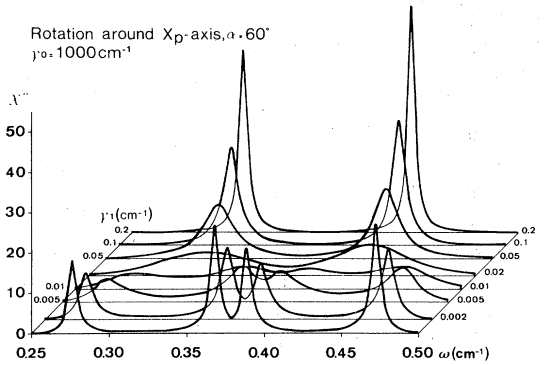

FIG. 15. ESR line shape for values of γ_1 between 10^{-3} and 0.2 cm^{-1} and for $\gamma_0 = 1000\ cm^{-1}$. The other parameters are the same as in Fig. 2(a).

at $\mathrm{Im}(R) \approx 0.42$ and 0.32 cm^{-1}, respectively. The real parts of these eigenvalues split, and two of them decrease with increasing values of γ_1, describing the narrowing of the ESR lines. This behavior of the ESR lines may be interpreted as a motional narrowing and will be discussed in more detail in Sec. IV.

IV. DISCUSSION

For a more qualitative discussion of the results of Sec. III, and laying stress upon the influence of the exciton motion on the ESR line shape, the equation of motion for the density operator without the spin degrees of freedom is considered here. In a basis $|n\rangle$, where $n = \{1, 2\}$ denotes whether the exciton is at the A or B molecule of the pair, from (A1.21) we arrive at the following set of equations[51,52]:

$$\dot{\rho}_{11} = -2\gamma_1(\rho_{11} - \rho_{22}) - iJ(\rho_{21} - \rho_{12}), \tag{4.1a}$$

$$\dot{\rho}_{22} = -2\gamma_1(\rho_{22} - \rho_{11}) + iJ(\rho_{21} - \rho_{12}), \tag{4.1b}$$

$$\dot{\rho}_{12} = -2(\gamma_0 + \gamma_1)\rho_{12} + 2\gamma_1\rho_{21} - iJ(\rho_{22} - \rho_{11}), \tag{4.1c}$$

$$\dot{\rho}_{21} = -2(\gamma_0 + \gamma_1)\rho_{21} + 2\gamma_1\rho_{12} + iJ(\rho_{22} - \rho_{11}). \tag{4.1d}$$

As we shall see this form of the equation is more suitable, when the strength of the local fluctuations γ_0 assumes large values. For small fluctuations γ_0 and γ_1, however, it is more convenient to represent the equations of motion in the basis formed by the Davydov states, which are solutions of the Schrödinger equation (3.6) without the spin terms and are given by

$$|+\rangle = (1/\sqrt{2})(|1\rangle + |2\rangle), \quad |-\rangle = (1/\sqrt{2})(|1\rangle - |2\rangle). \tag{4.2}$$

The set of equations (4.1) then transforms into

$$\dot{\rho}_{++} = -\gamma_0(\rho_{++} - \rho_{--}), \tag{4.2a}$$

$$\dot{\rho}_{--} = -\gamma_0(\rho_{--} - \rho_{++}), \tag{4.2b}$$

$$\dot{\rho}_{+-} = -(\gamma_0 + 4\gamma_1 + i2J)\rho_{+-} + \gamma_0\rho_{-+}, \tag{4.2c}$$

$$\dot{\rho}_{-+} = -(\gamma_0 + 4\gamma_1 - i2J)\rho_{-+} + \gamma_0\rho_{+-}. \tag{4.2d}$$

With the ansatz $\rho(t) = e^{St}\rho(0)$, the set of differential equations (4.1) or (4.2) transforms to an eigenvalue problem with the eigenvalues

$$S_1 = 0, \tag{4.3a}$$

$$S_2 = -2\gamma_0, \tag{4.3b}$$

$$\left.\begin{matrix} S_3 \\ S_4 \end{matrix}\right\} = -(\gamma_0 + 4\gamma_1) \pm i(4J^2 - \gamma_0^2)^{1/2}. \tag{4.3c, 4.3d}$$

The consideration of the corresponding eigenvectors shows that S_1 describes the stationary state and S_2 the decay of the nondiagonal elements of the density matrix [in the basis of (4.1)]. S_3 and S_4 are responsible for the time dependence of the motion of the excitation between the A and B molecules. As long as γ_0 is smaller than $2J$, S_3 and S_4 have an imaginary part describing an oscillatory motion of the exciton between the two sites. In this case the exciton motion may be denoted as coherent. For $\gamma_0 > 2J$ all eigenvalues are purely real and we obtain an exponential decay of the occupation numbers of the exciton; the exciton motion is in this case denoted as incoherent. Finally, it may happen that γ_0 is small, but $4\gamma_1$ is of the order of magnitude of the frequency of the motion. In this case the oscillatory behavior cannot be observed, and we denote the exciton motion as overdamped.

For large enough values of γ_0, phase relations between the two sites of the molecular pair decay rapidly and therefore the nondiagonal terms ρ_{12} and ρ_{21} in (4.1a) and (4.1b) may be neglected. In

this case it is obvious that $2\gamma_1$ is the hopping rate between the two molecules in the pair. From (4.2) we see that the density-matrix equations in the coherent-state representation decay into two separate sets of equations for the diagonal and nondiagonal elements. [The coupling between the two sets is introduced by the spin-orbit interaction in the Hamiltonian of (2.8).] Equations (4.2a) and (4.2b) then show that γ_0 is the hopping rate between the states of the upper and lower Davydov components.

After these preliminary remarks we consider Fig. 7. For small values of γ_0 we have two $\Delta m = 1$ ESR lines (besides the other two at $\omega \approx 4600$ G) at $\omega_1 \approx 3440$ G and at $\omega_2 \approx 3436$ G corresponding to transitions between E_3 and E_5 and between E_4 and E_6 in the upper and lower Davydov components. With increasing values of γ_0 the two lines broaden and coalesce for $\gamma_0 = 2$ G, i.e., $2\gamma_0 = \omega_1 - \omega_2$. For still larger values of γ_0 the single line becomes smaller. This situation may be described as a motional narrowing, where the spin does not move between different sites, but is scattered between the two Davydov states with a scattering rate γ_0 as described in (4.2a) and (4.2b). This limiting case of our model has been treated by van't Hof and Schmidt.[34] However, in this motional narrowing picture the broadening of the ESR lines and the splitting into four lines for still larger values of γ_0 (Fig. 8) cannot be explained; in order to discuss these effects, the whole 36×36 density matrix has to be considered.

The other limiting case of the completely incoherent exciton motion is shown in Fig. 15 for $\gamma_0 = 1000$ cm^{-1}. For very small values of γ_1 we have the four ESR lines corresponding to $\Delta m = 1$ transitions in the A and B molecules (see Table IV). If $4\gamma_1 \approx 0.08$ cm^{-1} and thus equals the difference in the line positions of corresponding ESR transitions in the two molecules, the lines merge into a single line which narrows when γ_1 increases further. This is exactly the usual case of motional narrowing, where the excitation hops between the two molecules as described in (4.1a) and (4.1b), if the nondiagonal terms ρ_{12} and ρ_{21} may be neglected.

The situation is similar in Figs. 13 and 14, where $\gamma_0 \gg 2J$ and the exciton motion is therefore incoherent. In Figs. 9 to 12, however, $\gamma_0 \ll 2J$, and if γ_1 is small too, we have the coherent exciton motion. With increasing values of γ_1 the damping parts of the eigenvalues S_3 and S_4 in (4.3) increase. For $\gamma_1 = 0.5$ cm^{-1} (≈ 5000 G), i.e., $4\gamma_1 = 2$ cm^{-1}, the damping part of the eigenvalues has the same magnitude as the oscillatory part, and we have now the situation that previously has been denoted as overdamped. When γ_1 increases further, the narrowing of the ESR lines starts.

In our calculation we have described the exciton motion within the Haken-Strobl model, which takes into account the influence of the phonons in a stochastic manner. This has the consequences that in the stationary state of the model all energy levels in the upper and lower Davodov components are populated with the same occupation probability, whereas in the real crystal we have a Boltzmann distribution. Taking this into account, we expect for $kT < 2J$ the contribution to the ESR spectrum of the transitions between E_3 and E_5 at 3440 G in the upper Davydov component to be weaker than that of the transition between E_4 and E_6 at 3436 G in the lower Davydov component (see Fig. 7). The details of the transition in Fig. 7 from the two lines to the single averaged line will therefore depend on how γ_0 and the Boltzmann-factor increase with temperature. For $kT > 2J$, however, the calculations should directly apply to experimental situations.

ACKNOWLEDGMENT

The author wishes to thank Dr. H. D. Vollmer for advice concerning the plotter evaluation of the computer data for the line shapes.

APPENDIX A: EQUATION OF MOTION FOR THE DENSITY OPERATOR

Here we give a concise derivation of the equation of motion for the density operator of a system, whose Hamiltonian consists of a time-independent part H_0 and of a stochastically time-dependent part $H_1(t)$,

$$H = H_0 + H_1(t) . \tag{A1.1}$$

In the Haken-Strobl model for the coupled coherent and incoherent motion of excitons $H_1(t)$ is given by

$$H_1(t) = \sum_{n,n'} h_{nn'}(t) b_n^\dagger b_{n'} , \tag{A1.2}$$

where $h_{nn'}(t)$ is a δ-correlated Gaussian stochastic process with disappearing mean value, and $b_n^\dagger$ and b_n are creation and annihilation operators for an electron-hole pair localized at site n.

The equation of motion for the density operator $\tilde{\rho}$ may be written in the following way:

$$\dot{\tilde{\rho}} = -i[H, \tilde{\rho}] = -iL\tilde{\rho} ; \tag{A1.3}$$

the Liouville operator L may be split into two terms in the same way as the Hamiltonian (A1.1):

$$L = L_0 + L_1(t) . \tag{A1.4}$$

Introducing the interaction picture by

$$\tilde{\rho}(t) = e^{-iL_0 t} \tilde{\rho}_I(t) , \tag{A1.5}$$

we arrive at the following equation of motion for $\tilde{\rho}_I(t)$:

$$\dot{\tilde{\rho}}_I(t) = -iL_{1I}(t) \tilde{\rho}_I(t) , \tag{A1.6}$$

with

$$L_{1I}(t) = e^{iL_0 t} L_1(t) e^{-iL_0 t} . \tag{A1.7}$$

The solution of this equation is given by

$$\tilde{\rho}_I(t) = T \exp\left(-i \int_0^t dt' \, L_{1I}(t')\right) \rho(0) , \tag{A1.8}$$

where T is the time-ordering operator. We now introduce a generalized density operator by

$$\tilde{\rho}_I[\alpha(t), t] = T \exp\left(-i \int_0^t dt' \, \alpha(t') \, L_{1I}(t')\right) \rho(0) , \tag{A1.9}$$

and using the functional derivative with respect to $\alpha(t)$, the equation of motion (A1.6) may be written

$$\dot{\tilde{\rho}}_I = 2[\delta/\delta\alpha(t)] \tilde{\rho}_I[\alpha(t), t]\big|_{\alpha(t)\equiv 1} . \tag{A1.10}$$

We are not interested in the quantity $\tilde{\rho}(t)$ containing the fluctuations, but in quantity $\rho(t)$ averaged over the fluctuations. Denoting this averaging procedure by the operator P, projecting out the fluctuations, we have

$$\rho(t) = P\tilde{\rho}(t) = e^{-iL_0 t} P \tilde{\rho}_I(t) = e^{-iL_0 t} \rho_I(t) . \tag{A1.11}$$

From (A1.10) we arrive at the equation of motion for $\rho_I(t)$:

$$\dot{\rho}_I(t) = P\dot{\tilde{\rho}}_I = 2[\delta/\delta\alpha(t)] P \tilde{\rho}_I[\alpha(t), t]\big|_{\alpha(t)\equiv 1} . \tag{A1.12}$$

Using the properties of the stochastic process $h_{nn'}(t)$, the density operator in the interaction picture (A1.9) may be written

$$P\tilde{\rho}_I[\alpha(t), t] = TP \exp\left(-i \int_0^t dt' \, \alpha(t') L_{1I}(t')\right) \rho(0) = T \exp\left(-\frac{1}{2} \int_0^t dt_1 \int_0^t dt_2 \, k_2(t_1, t_2) \alpha(t_1) \alpha(t_2)\right) \rho(0) , \tag{A1.13}$$

where the cumulant $k_2(t_1, t_2)$ is given by

$$k_2(t_1, t_2) = P L_{1I}(t_1) L_{1I}(t_2) = 2 \sum_{n, n'} \sum_{n'', n'''} \Lambda(n, n', n'', n''') \delta(t_1 - t_2) L_{1Inn'}(t_1) L_{1In''n'''}(t_2) . \tag{A1.14}$$

In the last part of Eq. (A1.14) the explicity expression for $L_1(t)$, i.e., for $H_1(t)$ according to (A1.2), has been used. Carrying through the functional derivative with respect to $\alpha(t)$ in (A1.13), we have

$$2 \frac{\delta}{\delta\alpha(t)} P\tilde{\rho}_I[\alpha(t), t]\big|_{\alpha(t)\equiv 1} = -T\left(\int_0^t dt_1 \int_0^t dt_2 \, k_2(t_1, t_2) \delta(t - t_1) \alpha(t_2) + \int_0^t dt_1 \int_0^t dt_2 k_2(t_1, t_2) \delta(t - t_2) \alpha(t_1) \right) \times \exp\left(-\frac{1}{2} \int_0^t dt_1 \int_0^t dt_2 \, k_2(t_1, t_2) \alpha(t_1) \alpha(t_2)\right) \rho(0) . \tag{A1.15}$$

Applying the time ordering operator and using (A1.14) we arrive at

$$\dot{\rho}_I = -\sum_{n, n'} \sum_{n'', n'''} \tfrac{1}{2} \Lambda(n, n', n'', n''') [L_{1In''n'''}(t) L_{1Inn'}(t) + L_{1Inn'}(t) L_{1In''n'''}(t)] \rho(t) . \tag{A1.16}$$

In the Haken-Strobl model for $\Lambda(n, n', n'', n''')$ the following expression has been used:

$$\Lambda(n, n', n'', n''') = \gamma_{|n-n'|} [\delta_{nn''} \delta_{n'n'''} + \delta_{nn'''} \delta_{n'n''} (1 - \delta_{nn'})] . \tag{A1.17}$$

This expression fulfills the symmetry relation

$$\Lambda(n, n', n'', n''') = \Lambda(n'', n''', n, n') , \tag{A1.18}$$

and with it, the equation of motion may be written

$$\dot{\rho}_I = -\sum_{n, n'} \sum_{n'', n'''} \Lambda(n, n', n'', n''') L_{1Inn'}(t) L_{1In''n'''}(t) \rho_I(t) . \tag{A1.19}$$

Going back to the Schrödinger picture, we obtain the following equation of motion for the density operator:

$$\dot{\rho}(t) = -iL_0 \rho(t) - \sum_{n, n'} \sum_{n'', n'''} \Lambda(n, n', n'', n''') L_{1nn'} L_{1n''n'''} \rho(t) . \tag{A1.20}$$

This equation consists of a commutator describing the coherent motion and of a double commutator stemming from the fluctuating part of the Hamiltonian. In the Haken-Strobl model, where n denotes the localization

of the electron-hole pair, (A1.20) may be written in the following matrix notation:

$$\dot{\rho}_{nn'} = -i[H_0, \rho]_{nn'} - 2\Gamma\rho_{nn'} + 2\delta_{nn'}\sum_{n''}\gamma_{|n''-n|}\rho_{n''n''} + 2(1-\delta_{nn'})\gamma_{|n-n'|}\rho_{n'n}\,, \tag{A1.21}$$

$$\Gamma = \sum_{n'}\gamma_{|n-n'|}\,. \tag{A1.22}$$

In the two-molecule model, $n, n', n'' = \{1, 2\}$ and $\Gamma = \gamma_0 + \gamma_1$.

APPENDIX B: CORRELATION FUNCTION FOR THE ESR LINE SHAPE

We consider a system described by the Liouville operator L_s, which generally also contains damping terms. The influence of an external time-dependent perturbation is taken into account by the Liouville-operator L_p:

$$L_p\Omega = [H_p, \Omega] = -[A, \Omega]F\cos\omega t = -L_A\Omega F\cos\omega t\,. \tag{A2.1}$$

The equation of motion for the density operator of the system is

$$i\dot{\rho} = L\rho\,, \tag{A2.2}$$

with

$$L = L_s + L_p\,, \tag{A2.3}$$

and its solution may be written in the following way:

$$\rho(t) = T\exp\left(-i\int_{-\infty}^{t}L(t'')\,dt''\right)\rho(-\infty)\,. \tag{A2.4}$$

Expanding this expression up to linear terms in L_p and assuming that $\rho(-\infty) = \rho_0$ describes the equilibrium, we arrive at

$$\rho(t) = \rho_0 + iF\int_0^\infty d\tau\, e^{-iL_s\tau}L_A\rho_0\cos\omega(t-\tau)\,. \tag{A2.5}$$

The expectation value of an observable B,

$$\langle B(t)\rangle = \mathrm{Tr}B\rho(t) = \mathrm{Tr}B^\dagger\rho(t) \equiv (B, \rho(t)) \tag{A2.6}$$

is then given by

$$\langle B(t)\rangle = (B, \rho_0) + iF\int_0^\infty d\tau\,(B, e^{-iL_s\tau}L_A\rho_0)\cos\omega(t-\tau)\,. \tag{A2.7}$$

From this expression we obtain the imaginary part χ'' of the susceptibility χ, describing the response of an observable B on a perturbation A:

$$\chi''(\omega) = i\int_0^\infty d\tau(B, e^{-iL_s\tau}L_A\rho_0)\sin\omega\tau\,. \tag{A2.8}$$

Denoting by $\tilde{R}_i$ and ρ^i the eigenvalues and eigenoperators of L_s and by η^i the eigenoperators of $L_s^\dagger$, we may expand $L_A\rho_0$ according to

$$L_A\rho_0 = \sum_i c_i\rho^i\,, \tag{A2.9}$$

with

$$c_i = (\eta^i, L_A\rho_0)\,. \tag{A2.10}$$

Inserting this expansion into (A2.8), the susceptibility is given by

$$\chi''(\omega) = \frac{1}{2}\sum_i (B, \rho^i)(\eta^i, L_A\rho_0) \times\left(\frac{-1}{i(\omega-\tilde{R}_i)} + \frac{-1}{i(\omega+\tilde{R}_i)}\right). \tag{A2.11}$$

In the following we wish to derive a high-temperature version of (A2.8). To that end we assume that the Liouville operator of the system L_s consists of two parts:

$$L_s\Omega = L_0\Omega + L_1\Omega = [H_0, \Omega] + L_1\Omega\,, \tag{A2.12}$$

where H_0 describes the state of equilibrium and L_1 the relaxation into that state. Explicitly, we assume that ρ_0 is given by

$$\rho_0 = e^{-\beta H_0}\,,\quad \beta = (kT)^{-1}\,. \tag{A2.13}$$

Using this expression for ρ_0, from (A2.8), we get, in the high-temperature approximation,

$$\chi''(\omega) = -i\beta\int_0^\infty d\tau(B, e^{-iL_s\tau}L_AH_0)\sin\omega\tau \tag{A2.14}$$

$$= +i\beta\int_0^\infty d\tau(B, e^{-iL_s\tau}(L_sA - L_1A))\sin\omega\tau\,, \tag{A2.15}$$

$$= -\beta\int_0^\infty d\tau\frac{d}{d\tau}(B, e^{-iL_s\tau}A)\sin\omega\tau - i\beta\int_0^\infty d\tau(B, e^{-iL_s\tau}L_1A)\sin\omega\tau\,, \tag{A2.16}$$

$$= \beta\omega\int_0^\infty d\tau(B, e^{-iL_s\tau}A)\cos\omega\tau - i\beta\int_0^\infty d\tau(B, e^{-iL_s\tau}L_1A)\sin\omega\tau\,. \tag{A2.17}$$

Generally, L_1 consists of two parts L_{11} and L_{12}, from which the first one describes relaxation within the electronic degrees of freedom and the

second one relaxation within the spin system. If the operator A contains only spin degrees of freedom, the contribution from L_{11} vanishes exactly; if furthermore the relaxation rates in L_{12} are small enough, the second term in (A2.17) may be neglected, and $\chi''(\omega)$ is given by

$$\chi''(\omega) = \beta\omega \int_0^\infty d\tau (B, e^{-iL_s\tau}A) \cos\omega\tau . \tag{A2.18}$$

In the Haken-Strobl model the eigenoperator ρ^s describing the stationary solution ($\tilde{R}_s = 0$) is proportional to the unity operator. Using furtheron $\mathrm{Tr}\rho^i \propto \delta_{is}$, the expression for the susceptibility may be written

$$\chi''(\omega) \propto \beta\omega \sum_i \int_0^\infty d\tau (\eta^s, B^\dagger\rho^i)(\eta^i, A\rho^s) \times e^{-i\tilde{R}_i\tau} \cos\omega\tau . \tag{A2.19}$$

Calculating the integral and taking into account that the contribution of the term containing the stationary eigenvalue $\tilde{R}_s$ disappears because of $\omega\delta(\omega) = 0$, we arrive at

$$\chi''(\omega) = \frac{i}{N} \sum_i (\eta^s, B^\dagger\rho^i)(\eta^i, A\rho^s) \left(\frac{\omega}{\omega + \tilde{R}_i} - \frac{\omega}{\omega - \tilde{R}_i} \right) . \tag{A2.20}$$

The normalization constant N is determined from

$$\int_0^\infty \chi''(\omega)\, d\omega = 1 , \tag{A2.21}$$

and we have

$$N = \lim_{\alpha\to\infty} -i \sum_i (\eta^s, B^\dagger\rho^i)(\eta^i, A\rho^s) \times \int_0^\alpha \left(\frac{\tilde{R}_i}{\omega + \tilde{R}_i} + \frac{\tilde{R}_i}{\omega - \tilde{R}_i} \right) d\omega \tag{A2.22}$$

$$= \lim_{\alpha\to\infty} -i \sum_i (\eta^s, B^\dagger\rho^i)(\eta^i, A\rho^s)\tilde{R}_i \times [\ln(\alpha + \tilde{R}_i) - \ln\tilde{R}_i + \ln(\alpha - \tilde{R}_i) - \ln(-\tilde{R}_i)] . \tag{A2.23}$$

Expressing the eigenvalue $\tilde{R}_i$ by its real and imaginary parts

$$\tilde{R}_i = \tilde{\omega}_i - i\tilde{\gamma}_i , \tag{A2.24}$$

the square bracket in (A2.23) gives

$$\lim_{\alpha\to\infty} [\ln(\alpha + \tilde{\omega}_i - i\tilde{\gamma}_i) + \ln(\alpha - \tilde{\omega}_i + i\tilde{\gamma}_i) - \ln(\tilde{\omega}_i - i\tilde{\gamma}_i) - \ln(-\tilde{\omega}_i + i\tilde{\gamma}_i)]$$

$$= \lim_{\alpha\to\infty} \Bigg(\ln\left[[(\alpha + \tilde{\omega}_i)^2 + \tilde{\gamma}_i^2]^{1/2} \exp\left(-i \arctan\frac{\tilde{\gamma}_i}{\alpha + \tilde{\omega}_i} \right) \right] + \ln\left[[(\alpha - \tilde{\omega}_i)^2 + \tilde{\gamma}_i^2]^{1/2} \exp\left(-i \arctan\frac{\tilde{\gamma}_i}{\alpha + \tilde{\omega}_i} \right) \right] - \ln\left[(\tilde{\omega}_i^2 + \tilde{\gamma}_i^2)^{1/2} \exp\left(-i \arctan\frac{\tilde{\gamma}_i}{\tilde{\omega}_i} \right) \right] - \ln\left\{ (\tilde{\omega}_i^2 + \tilde{\gamma}_i^2)^{1/2} \exp\left[-i \arctan\left(\frac{\tilde{\gamma}_i}{\tilde{\omega}_i} - \pi \right) \right] \right\} \Bigg) , \tag{A2.25}$$

$$= \lim_{\alpha\to\infty} [2\ln\alpha - \ln(\tilde{\omega}_i^2 + \tilde{\gamma}_i^2) + 2i \arctan(\tilde{\gamma}_i/\tilde{\omega}_i) - i\pi] . \tag{A2.26}$$

The expressions in small square brackets without an index i give a constant factor to the sum of (A2.23); the evaluation of the sum in this case results in

$$\sum_i (\eta^s, B^\dagger\rho^i)(\eta^i, A\rho^s)\tilde{R}_i = (\eta^s, B^\dagger L_s A\rho^s) \propto \mathrm{Tr}(B^\dagger L_s A) . \tag{A2.27}$$

In the Haken-Strobl model, L_s consists of a commutator L_0 and a double commutator L_1 containing no spin operators. If $\chi''(\omega)$ describes the ESR line shape of triplet excitons, A and B are given by the spin operator M_x. In this case $L_1 A$ is zero, and the contribution of L_0 is zero too on account of

$$\mathrm{Tr}M_x[H_0, M_x] = \mathrm{Tr}H_0[M_x, M_x] = 0 . \tag{A2.28}$$

The normalization constant is then given by

$$N = \sum_i (\eta^s, B^\dagger\rho^i)(\eta^i, A\rho^s)(-i\tilde{R}_i) \times \left(-\ln(\tilde{\omega}_i^2 + \tilde{\gamma}_i^2) + 2i \arctan\frac{\tilde{\gamma}_i}{\tilde{\omega}_i} \right) . \tag{A2.29}$$

[1]J. Frenkel, Phys. Rev. 37, 17 (1931); 37, 1276 (1931).
[2]A. S. Davydov, *Theory of Molecular Excitons* (McGraw-Hill, New York, San Francisco, Toronto, London, 1962); and (Plenum, New York, London, 1971).
[3]D. Haarer and H. C. Wolf, Phys. Status Solidi B 33, K117 (1969).
[4]D. Haarer, thesis (University of Stuttgart, 1969) (unpublished).
[5]D. Haarer and H. C. Wolf, Mol. Cryst. Liquid Cryst. 10, 359 (1970).
[6]W. Bizzarro, J. Rosenthal, N. F. Berk, and L. Yarmus Phys. Status Solidi B 84, 27 (1977).
[7]P. Reineker, Phys. Status Solidi B 70, 189 (1975); 70, 471 (1975); 74, 121 (1976).
[8]P. Reineker, Z. Phys. B 21, 409 (1975).
[9]Tj. Hibma and J. Kommandeur, Phys. Rev. B 12, 2608 (1975).
[10]G. Castro and R. M. Hochstrasser, J. Chem. Phys. 47, 2241 (1967); 48, 637 (1968).
[11]R. M. Hochstrasser and J. D. Whiteman, J. Chem. Phys. 56, 5945 (1972).
[12]R. Schmidberger and H. C. Wolf, Chem. Phys. Lett. 16, 402 (1972).
[13]R. Schmidberger and H. C. Wolf, Chem. Phys. Lett. 25, 185 (1974).
[14]R. Schmidberger, thesis (University of Stuttgart, 1974) (unpublished).
[15]A. H. Francis and C. B. Harris, Chem. Phys. Lett. 9, 181 (1971); 9, 188 (1971); J. Chem. Phys. 55, 3595 (1971).
[16]M. D. Fayer and C. B. Harris, Phys. Rev. B 9, 748 (1974).
[17]C. B. Harris and M. D. Fayer, Phys. Rev. B 10, 1784 (1974).
[18]H. Sternlicht and H. M. McConnell, J. Chem. Phys. 35, 1793 (1961).
[19]M. S. de Groot, I. A. M. Hesselman, and J. H. van der Waals, Mol. Phys. 12, 259 (1967).
[20]R. M. Hochstrasser and A. H. Zweail, Chem. Phys. 4, 142 (1972).
[21]A. H. Zewail and C. B. Harris, Chem. Phys. Lett. 28, 8 (1974).
[22]A. H. Zewail and C. B. Harris, Phys.Rev. B 11, 935 (1975); 11, 952 (1975).
[23]H. Port (private communication).
[24]B. J. Botter, A. J. van Strien, and J. Schmidt, Chem. Phys. Lett. 49, 39 (1977).
[25]M. Schwoerer and H. C. Wolf, Proc. Colloq. AMPERE 14, 544 (1966).
[26]M. Schwoerer and H. C. Wolf, Mol. Cryst. 3, 177 (1967).
[27]C. A. Hutchison and B. W. Mangum, J. Chem. Phys. 34, 908 (1961).
[28]M. Schwoerer, thesis (University of Stuttgart, 1967) (unpublished).
[29]D. M. Hanson, J. Chem. Phys. 52, 3409 (1970).
[30]C. L. Braun and H. C. Wolf, Chem. Phys. Lett. 9, 260 (1971).
[31]Ph. Kottis, Chem. Phys. Lett. 6, 133 (1970).
[32]D. M. Hanson, Chem. Phys. Lett. 11, 175 (1971).
[33]B. J. Botter, C. J. Nonhof, J. Schmidt, and J. H. van der Waals, Chem. Phys. Lett. 43, 210 (1976).
[34]C. A. van't Hof and J. Schmidt, Chem. Phys. Lett. 36, 460 (1975).
[35]H. Hinkel, thesis (University of Stuttgart, 1977) (unpublished).
[36]H. Hinkel, H. Port, H. Sixl, M. Schwoerer, P. Reineker, and D. Richardt (unpublished).
[37]H. Haken and G. Strobl, in *The Triplet State*, edited by A. B. Zahlan (Cambridge U.P., Cambridge, England, 1967).
[38]H. Haken and P. Reineker, Z. Phys. 249, 253 (1972).
[39]H. Haken and G. Strobl, Z. Phys. 262, 135 (1973).
[40]R. E. Merrifield, J. Chem. Phys. 28, 647 (1958).
[41]M. Trlifaj, Czech. J. Phys. 8, 510 (1958).
[42]P. Avakian, V. Ern, R. E. Merrifield, and A. Suna, Phys. Rev. 165, 974 (1968).
[43]P. Reineker, Phys. Lett. A 44, 429 (1973).
[44]E. Schwarzer, thesis (University of Stuttgart, 1974) (unpublished).
[45]H. Haken and P. Reineker, in *Excitons, Magnons and Phonons*, edited by A. B. Zahlan (Cambridge U.P., Cambridge, England, 1968).
[46]M. K. Grover and R. Silbey, J. Chem. Phys. 52, 2099 (1969); 54, 4843 (1971).
[47]V. M. Kenkre and R. S. Knox, Phys. Rev. B 9, 5279 (1974).
[48]V. M. Kenkre and R. S. Knox, Phys. Rev. Lett. 33, 803 (1974).
[49]R. Zwanzig, in *Lectures in Theoretical Physics*, edited by W. E. Brittin, B. W. Downs, and J. Downs (Interscience, New York, 1961), Vol. III.
[50]V. M. Kenkre, Phys. Rev. B 11, 1741 (1975); 12, 2150 (1975).
[51]H. Haken and P. Reineker, Acta Univ. Carolinae–Mat. Phys. 14, 23 (1973).
[52]P. Reineker and H. Haken, in *Localization and Delocalization in Quantum Chemistry*, edited by O. Chalvet, R. Daudel, S. Diner, and J. P. Malrieu (Reidel, Dortrecht, Boston, 1976), Vol. II.
[53]R. Silbey, Ann. Rev. Phys. Chem. 27, 203 (1976).
[54]P. W. Anderson, J. Phys. Soc. Jpn. 9, 316 (1954).
[55]A. Hudson and A. D. McLachlan, J. Chem. Phys. 43, 1518 (1965).
[56]C. B. Harris and M. D. Fayer, Phys. Rev. B 10, 1784 (1974).
[57]G. O. Berim and A. R. Kessel, Phys. Status Solidi B 76, 827 (1976); 79, 489 (1977).
[58]P. Reineker, Phys. Status Solidi B 52, 439 (1972).
[59]P. Reineker, Solid State Commun. 14, 153 (1974).
[60]P. Reineker, Z. Naturforsch. A 29, 282 (1974).
[61]A. Carrington and A. D. McLachlan, *Introduction to Magnetic Resonance* (Harper and Row, New York, 1967).
[62]D. W. J. Cruickshank, Acta Crystallogr. 10, 504 (1957).
[63]D. Richardt, Staatsexamensarbeit (University of Ulm, 1976) (unpublished).
[64]P. Reineker and D. Richardt (unpublished).
[65]J. Grad and M. A. Brebner, in Collected Algorithms from CACM, Algorithm 343 (unpublished).
[66]J. H. Wilkinson, *The Algebraic Eigenvalue Problem* (Clarendon, Oxford, 1965).
[67]D. Richardt and P. Reineker (unpublished).
[68]A. Abragam, *The Principles of Nuclear Magnetism* (Clarendon, Oxford, 1970).